Investigation of the Influence of Roughness on the Shear Resistance of Concrete-Rock Interfaces Using Random Field Simulations, Numerical Simulations, and Neural Network Modeling: Proposition of Two Approaches for the Estimation of the Peak Shear Strength

Menes Badika, Sophie Capdevielle, Dominique Saletti, Matthieu Briffaut

Investigation of the influence of roughness on the shear resistance of concrete-rock interfaces using random field simulations, numerical simulations, and neural network modeling: proposition of two approaches for the estimation of the peak shear strength

Menes Badika[1,*], Sophie Capdevielle[1], Dominique Saletti[1]and Matthieu Briffaut[2]

1 Univ. Grenoble Alpes, CNRS, Grenoble INP - UGA, 3SR, Grenoble, France; menes.badika@irsn.fr(MB), sophie.capdevielle@univ-grenoble-alpes.fr (S.C.); dominique.saletti@univ-grenoble-alpes.fr (D.S.),

2 Laboratoire de Mécanique, Multiphysique, Multiéchelle-LaMcube-UMR 9013, CNRS, Centrale Lille, University Lille, 59000 Lille, France; matthieu.briffaut@centralelille.fr (M.B.)

* Correspondence: sophie.capdevielle@univ-grenoble-alpes.fr

Highlights

- New methodology to investigate the influence of roughness on the shear behavior of interfaces
- Methodology to generate databases of synthetic rough rock surfaces with controlled roughness values
- Establishment of numerical simulations as a strategy to perform extensive virtual experimental studies
- The correlation between interface roughness and shear strength is not bijective.
- Assessment of artificial neural network modeling as a complementary alternative to failure criteria

Abstract

This paper presents a new approach to determine more robust shear failure criteria, focusing on rough concrete-rock interfaces. The proposed method could also be applied to rock joints. The new approach is based on the distribution and variety of interfaces numerically tested in terms of surface roughness. For this reason, random field simulations are performed using the turning bands method to generate an extensive database of synthetic rough rock surfaces. With this database of synthetic rough rock surfaces, numerical simulations of direct shear tests are carried out. Finally, analytical and neural network models are proposed using the database of shear strength obtained from the finite element simulations to estimate the peak shear strength of concrete-rock interfaces. The performances of the analytical and neural network models in estimating this peak shear strength are evaluated by computing the percentage error and the mean absolute error (MAE) between the predicted and the numerically obtained values. Both models lead to satisfactory predictions. Nevertheless, it is worth noting that the neural network model mildly outperforms the analytical model regarding the magnitude of the error. Furthermore, the neural network model reproduces the possible non-bijective aspect of the correlation roughness-peak shear strength.

Keywords: roughness, peak shear strength, random field simulation, numerical simulation, analytical model, neural network model.

List of Symbols

$\gamma(h)$	Theoretical variogram function
$Z(x)$	Random function
$x\ and\ x+h$	Pairs of points in a certain domain separated by a distance equivalent to h
$m(h)$	The mean or drift
$C(h)$	Covariance function
$E[\square]$	Mathematical expectation (linear operator)
$var[\square]$	Variance of a random variable
$2\gamma(h)$	Variance of a random variable
$C_{sph}(h)$	Covariance function: spherical model
a	Variogram range
b	Variogram sill
$z_s(X)$	3D realization obtained using a turning bands method
N_l	Number of lines in one-dimensional simulation of the turning bands method

$z_i(<\overrightarrow{OX_\iota}, \overrightarrow{u_\iota}>)$	Realization of the turning bands method (1D)
N_l	Number of lines: turning bands method (1D)
$C_3(r)$	Three-dimensional covariance function
$C_1(r)$	Uni-dimensional covariance function
$\frac{d}{dx}$	Differentiation operator
$\theta^*_{max}/(C+1)$	Grasselli roughness parameter
k_n	Normal stiffness
k_s	Shear stiffness
σ°	Normal strength
τ°	Shear strength
$\delta_B - \delta_C$	Shear displacement
α	Damage parameter
μ	Friction coefficient
τ_p	Peak shear strength
σ_n	Normal stress
τ	Shear stress
ϕ_b	Basic friction angle
A_0	Maximum contact area during shear
σ_t	Tensile strength
c	Cohesion
f_{NN}	Neural network function
τ_{NN}	Neural network predicted peak shear strength
MSE	Mean squared error
MAE	Mean absolute error
n	Number of points considered in MAE and MSE
u	Shear displacement
u_m	Shear displacement until contact between the two slabs in a direct shear test
τ_r	Residual shear strength
u_p	Peak shear displacement
Δu_p	Horizontal displacement before the peak
δ_{si}	Shear displacement at time i
τ_{si}	Shear stress at time i

1. Introduction

The shear behavior of interfaces is one of the most investigated subjects in rock mechanics. Since the early fifties, the investigation of the shear behavior of interfaces culminates each year in dozens of scientific communications (Patton 1966; Bandis, Lumsden, and Barton 1981; Grasselli and Egger 2003; Saiang, Malmgren, and Nordlund 2005; Moradian et al. 2010; Moradian, Ballivy, and Rivard 2012; Tian et al. 2015; Mouzannar et al. 2017) It is today accepted that, within the range of normal stress useful for most geotechnical problems, the shear behavior of rock-rock and concrete-rock interfaces are mainly influenced by the cohesion, the normal stress, the geometrical properties of the interface, the roughness, and the basic friction angle. Despite this interest and the achievements in this area, it seems that the research for more robust failure criteria linking the most influential parameters of the shear behavior to the peak shear strength is still ongoing (Patton 1966; Ladany and Archambault 1969; Barton and Choubey 1977; Hoek

and Brown 1980; Plesha 1987; Amadei et al. 1998; Grasselli and Egger 2003; Liu et al. 2017). In particular, the influence of roughness in the shear behavior still needs more investigation.

Most studies are usually based on a handful of rough rock surfaces that hardly encompass a more comprehensive range of roughness encountered in nature. This shortcoming is overcome in the present research by considering the number and variety of rough rock surfaces. Many parameters have been proposed to quantify the roughness of rock surfaces to estimate the peak shear strength. These roughness parameters are separated into two main groups, the 2D roughness parameters (El-Soudani 1978; Myers 1962; Whitehouse 2023; Barton and Choubey 1977) and the 3D roughness parameters (El-Soudani 1978; Grasselli and Egger 2003; Bryan S. A. Tatone and Grasselli 2009). Of all these parameters, the JRC (Barton and Choubey 1977) and the $\theta^*_{max}/(C+1)$ (Bryan S. A. Tatone and Grasselli 2009) are of particular interest in the problem of the estimation of the shear resistance of a rough interface. The JRC is based on extensive experimental studies and back-calculation analysis. On the other hand, $\theta^*_{max}/(C+1)$ has a straightforward geomechanical rationale. In this paper, the focus is on understanding the influence of roughness as a three-dimensional entity on the shear resistance of concrete-rock interfaces under low normal loading (e.g: mid-height concrete gravity dams and rock support systems on shallow excavation); this means that only the 3D roughness parameter $\theta^*_{max}/(C+1)$ (Bryan S. A. Tatone and Grasselli 2009) is used. Collecting rough rock surfaces with specified roughness values is experimentally very challenging. For this reason, it is essential to define a methodology to generate artificially synthetic rough rock surfaces. Random field simulation is an example of such a methodology. Random field simulation has been recently used to generate synthetic rough rock surfaces. Casagrande et al. (Casagrande et al. 2018) performed random field simulations to generate synthetic rough rock surfaces to estimate the shear strength of rock-rock interfaces using a stochastic approach. Jeffery et al.(Jeffery et al. 2021) improved the rigor of the methodology proposed by Casagrande et al. (Casagrande et al. 2018). The new methodology consists of transforming a 2D trace of a discontinuity into three daughter profiles, performing the random field simulations using, as input, the parameters of each daughter profile, and superposing the results of the three simulations into a single profile, which is then used to obtain one 3D realization. Both Casagrande et al. (Casagrande et al. 2018) and Jeffery et al. (Jeffery et al. 2021) use the local average subdivision algorithm (LAS) (Fenton and Vanmarcke 1990) to perform random field simulations. Although this methodology is quite useful when only the trace of a rough rock surface is accessible, it still suffers from the limitation of characterizing the roughness of rock surfaces using a single two-dimensional profile. In this study, however, the turning bands method is selected to perform random field simulations using the three-dimensional geostatistics characteristics of rough rock surfaces.

Even with a rich database of synthetic rough rock surfaces, it is still complex to properly assess the influence of roughness on the shear behavior of interfaces. This complexity is caused by the challenge of performing many reliable and repeatable experimental tests. For this reason, numerical simulations of direct shear tests are ideal to investigate the influence of roughness on the shear behavior of interfaces once the numerical model is validated by experimental results. Progress has been made on the numerical modeling of the shear behavior of concrete-rock interfaces. Badika et al. (Badika et al. 2022), Tian et al. (Tian et al. 2015), and Zhao et al. (Zhao, Chen, and Zhao 2018) used the cohesive-frictional model to simulate direct shear tests of concrete rock interfaces using the rough concrete-granite, smooth concrete-dolomite, and foamed concrete-sandstone interfaces. This model is appropriate for investigating the shear behavior of concrete-rock interfaces under low normal loading. Specifically, the calibrated and validated model presented by Badika et al. (Badika et al. 2022) for bonded rock-concrete interfaces is used to simulate the direct shear tests performed in the present paper.

With a sufficiently large database of shear history representing the numerical simulations of direct shear tests of synthetic rough rock surfaces, it might be possible to propose more robust failure criteria. The general approach to define a failure criterion is to define an analytical model based on the interpretation and understanding of the underlying mechanisms active during the shear process (Grasselli and Egger 2003; Barton and Choubey 1977; Patton 1966; Ladany and Archambault 1969). This approach is one of the two approaches adopted in this research. The other approach is to associate the understanding of the shear mechanisms active during shear with the computational capability to recognize complex statistical patterns within the database of shear strength. In this second approach, a failure criterion is based on artificial neural network modeling that can perform the same task as the analytical model. Artificial neural networks (ANN) application in rock mechanics research has grown substantially in the last twenty years. This growth has been fueled by the availability of powerful computers and data usually collected for mining

engineering projects (Delavar and Ramezanzadeh 2023; Khandelwal and Singh 2009) and the advances in machine learning research overall (Krizhevsky, Sutskever, and Hinton 2017). The advances in machine learning have positioned artificial neural network models as a possible alternative to numerical simulations (Furtney et al. 2022), analytical models(Dantas Neto et al. 2017), and or experimental studies (Sakaridis, Karathanasopoulos, and Mohr 2022; Furtney et al. 2022). Furthermore, ANN models have been used extensively to estimate the rock properties, such as the compressive strength of rock(Furtney et al. 2022; Meulenkamp and Grima 1999; Rabbani et al. 2012; Yesiloglu-Gultekin, Gokceoglu, and Sezer 2013; Jahed Armaghani et al. 2016; Rajesh Kumar et al. 2013), elastic modulus (Rajesh Kumar et al. 2013), and the major principal stress(Rukhaiyar and Samadhiya 2017).

In this paper, random field simulations are carried out using the turning bands method to generate an extensive database of synthetic rough rock surfaces. Finite element simulations of direct shear tests of concrete-rock interfaces are performed using the database of synthetic rough rock surfaces. The results of these numerical simulations yield a database of shear strength. This database of shear strength is then used to propose two methodologies to estimate the peak shear strength of concrete-rock interfaces.

2. Generation of synthetic rough rock surfaces

The generation of synthetic rough rock surfaces proceeded in three main steps (Fig. 1). First, the fields of heights of asperities representing each interface tested are normalized. Second, the normalized data obtained is used in the variogram analysis, yielding parameters characterizing each field in terms of spatial correlation and variance. Last, these characteristic parameters are used as inputs of random field simulations to generate synthetic rough rock surfaces. More details about each of the steps are presented later.

For the generation of synthetic rough rock surfaces in this study, roughness data collected by El Merabi (El Merabi 2018) was used. This data was obtained by scanning rough granite blocks used to generate bonded concrete-rock samples. These samples were used to perform direct shear tests as part of an extensive experimental study designed to investigate the influence of roughness on the shear behavior of concrete-rock interfaces.

2.1 The roughness of rough rock surfaces as a random function

Every field of heights of asperities representing a rough rock surface is a dataset that maintains the concept of regionalization since each field value is correctly associated with a specific location in a physical space and maintains a correlation with other heights of asperities located in its surroundings. Moreover, it is very challenging to define a deterministic function that fits all the heights of asperities composing the field. Therefore, a probabilistic approach to characterize the field of heights of asperities is more suitable. Furthermore, the probabilistic approach introduces the concepts of randomness, such as each field value can be envisioned as a result of a random mechanism. Therefore, the association of regionalization and randomness is the base of the definition of random function (Wackernagel 2003). This association means that the roughness of rough rock surfaces can be considered a random function. Consequently, the random field theory can be used to simulate synthetic rough rock surfaces. The process of the random field simulation to generate synthetic rough rock surfaces is displayed in Fig. 1. The detailed method to statistically analyze the roughness data (steps 1 to 3) is explained in section 2.2. The random field simulation (step 4) is further developed in section 2.3. Eventually, the complete process applied to the generation of the synthetic rock surfaces for the present research is described in section 2.4.

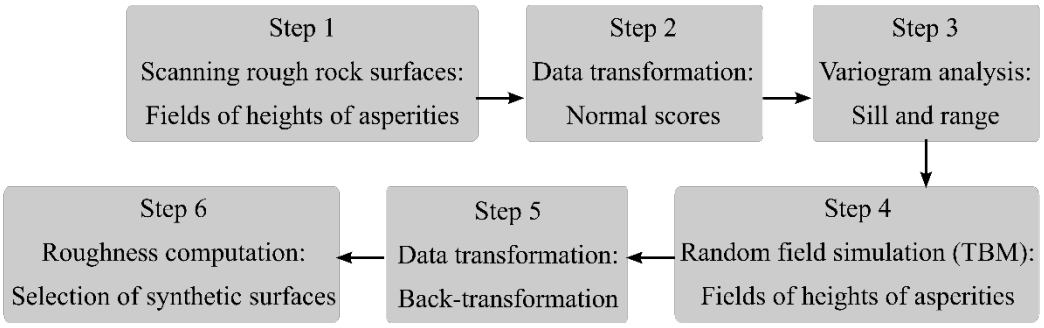

Fig. 1 Synthetic rough rock surface generator using random field simulation

2.2 Statistical and geostatistical data processing

The methodology for simulating random fields in this work requires the data to be normally distributed. Unfortunately, the distribution of heights of asperities constituting the rough rock surface, as many other properties of interest in rock and soil mechanics, do not automatically follow a normal (or Gaussian) distribution (Fenton and Griffiths 2008; Casagrande et al. 2018). Therefore, the quantile-to-quantile normal score transformation is used to normalize the distribution of heights of asperities (Deutsch and Journel 1998; Pyrcz and Deutsch 2020). An illustration of this transformation for one rough granite surface is presented in Fig. 2.

A further requirement for the simulation of random functions using the random field theory is that the statistical characteristics of the first and the second moment (mean and variance) must remain constant within the domain. This requirement is the consideration of stationarity. In this research, the intrinsic stationarity hypothesis is used. This hypothesis means that the stationarity has to be satisfied only for the sums of differences between pairs of points, leading to the concept of variogram (Wackernagel 2003).

A variogram function is an expression of the dissimilarity between pairs of points x and $x + h$ and is computed using Eq. (1).

$$\gamma(h) = \frac{1}{2} E[(Z(x+h) - Z(x))^2] \qquad (1)$$

where $E[\,]$ is the mathematical expectation.

In this research, the interest is in the generation of fields of correlated data. For this reason, the expression of similarity is more desired than the expression of dissimilarity. Consequently, the covariance function is used in the random field simulation instead of the variogram function.

The covariance function is defined based on the concept of intrinsic stationarity of the two first moments (mean $E[\,]$ and variance $var[\,]$) of a random function $Z(x)$, see Eq. (2) and Eq. (3).

$$E[Z(x+h) - Z(x)] = m(h) = 0 \qquad (2)$$

$$var[Z(x+h) - Z(x)] = 2\gamma(h) \qquad (3)$$

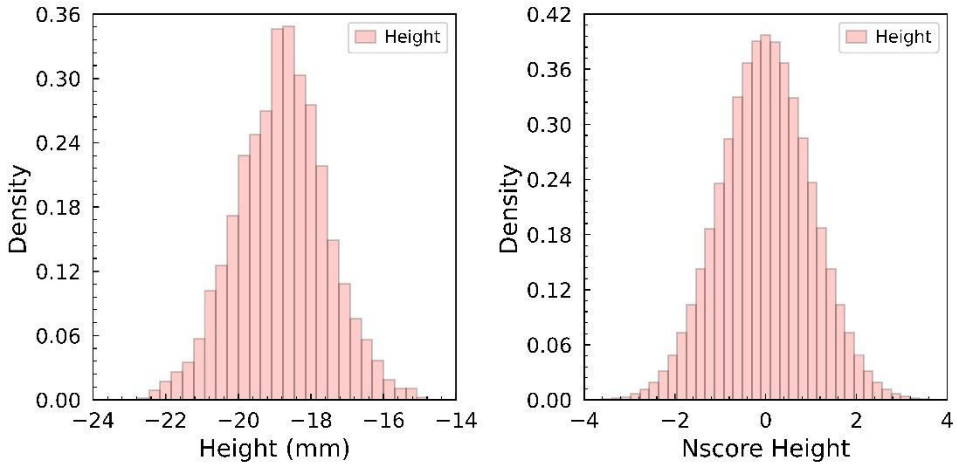

Fig. 2 Data transformation: the nscores obtained are the normalized distribution of heights of asperities of a rough granite surface (step 2 of the synthetic rock surface generation process)

For all points x and $x + h$, the covariance function is defined according to Eq. (4).

$$E[Z(x)\,Z(x+h)] - (E[Z(x)])^2 = C(h) \qquad (4)$$

The variogram function can be computed using the covariance function;

$$\gamma(h) = C(0) - C(h) \qquad (5)$$

The covariance function used in this research is the spherical model, Eq. (6). This model is selected because it best fits the shape of point cloud values obtained after calculating variograms of rough granite surfaces. The quality of fitting the covariance function to the shape of the variogram points calculated is important because these functions are designed to capture the general characteristics of a field. Using covariance functions instead of simple variogram points is necessary to add a physical meaning to the characterization of a field (Wackernagel 2003).

$$C_{sph}(h) = \begin{cases} b\left(1 - \frac{3}{2}\frac{|h|}{a} + \frac{1}{2}\frac{h^3}{a^3}\right) & for\ 0 \le |h| \le a \\ 0 & for\ |h| > a \end{cases} \qquad (6)$$

where a represents the range and b represents the sill.

The spherical covariance function is defined using three parameters: the nugget effect, the range, and the sill. The nugget effect is associated with the unreliable variation of variogram values when smaller distances between pairs of points are considered. According to Eq. (1), this means smaller values of h. This parameter is not considered in the present study because the rough granite surfaces used in the variogram analysis are small and well-sampled. The range a is the distance between pairs of points at which the values of the variograms begin to stabilize. The variogram value when the range a is reached is called the sill b. The range a is an expression of the correlation distance between the points of a field. The sill b can be interpreted differently depending on the geostatistical context. In this study, the sill is an expression of the variance of the data used in the computation of variograms. Since all the data are normalized, the sill is limited to one. This consideration can be interpreted as if the variogram values are above the sill, the data are inversely correlated. The data are directly correlated if the variograms are below the sill (Samson and Deutsch

2021). The range a and the sill b are used as the inputs of the random field simulations aiming at reproducing the correlation between the points with controllable variance.

In this study, the fields of heights of asperities obtained by scanning rough granite surfaces are first normalized, then the normalized data obtained is used to compute variograms. The variogram points are fitted to a spherical covariance function defining the range a and the sill b. The range a and the sill b obtained are used in the random field simulation presented hereafter to obtain new synthetic rough rock surfaces with similar correlation distance and controllable variance.

The simulation of random fields, as implemented in this research, is restricted to isotropic random fields; this means that the covariance function is assumed to be constant independently of the direction of the vector h.

Fig. 3 shows the result of a variogram analysis of a natural rough granite surface in two directions, yielding two combinations of sill and range (covariance parameters) used as input for two random field simulations: (1, 25) and (1, 20).

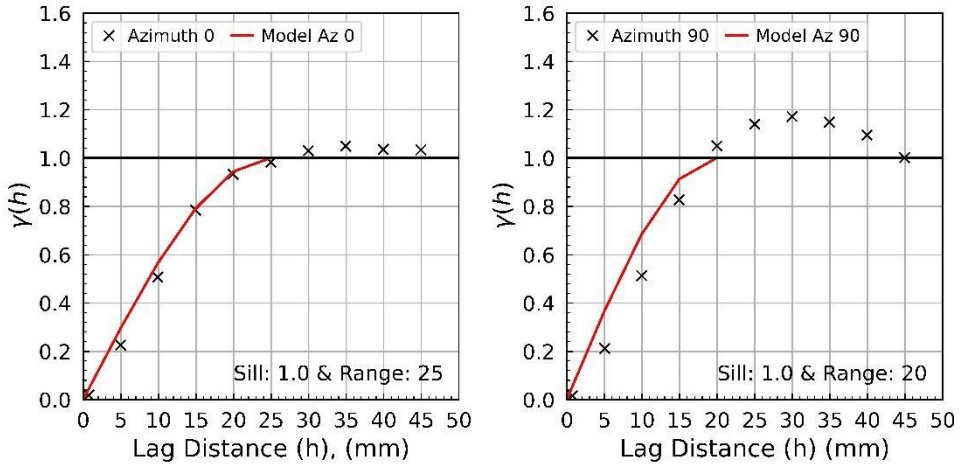

Fig. 3 Variogram analysis of rough rock surfaces (step 3 of the synthetic rock surface generation process)

2.3 Simulation of random fields using the turning band method

Random field simulations are carried out using as inputs the range a and the sill b of spherical covariance functions used to fit the variograms computed using the points cloud representing the heights of asperities of rough granite surfaces. The outputs obtained in these simulations are fields of heights of asperities denominated synthetic rough rock surfaces. These synthetic rough rock surfaces have geostatistical characteristics (range a and sill b) within an acceptable range of the ones of the input of the random field simulation. Synthetic rough rock surfaces with defined roughness values are then selected from the database of synthetic rough rock surfaces generated.

This research uses the turning bands method to perform random field simulations. This method has a solid geostatistical background and uses variogram analysis. A summary of the method is provided below. A more detailed presentation of the turning bands methods can be found in the literature (Chilès and Delfiner 2012; Journel and Huijbregts 1976; Mantoglou and Wilson 1982; Matheron 1973).

The turning bands method reduces two-dimensional and three-dimensional problems into unidimensional ones. Consequently, instead of performing three-dimensional simulations straight away, a series of unidimensional simulations are carried out along a set of lines. Then, a single regionalized value of a realization is obtained using the projected values in the unidimensional realizations according to Eq. (7).

$$z_s(X) = \frac{1}{\sqrt{N_l}} \sum_{1}^{N_l} z_i(< \overrightarrow{OX_\iota}, \overrightarrow{u_\iota} >) \qquad (7)$$

Where N_l, the number of lines and the subscript s indicates the simulated synthetic value.

The direct relationship between the three-dimensional covariance function and the unidimensional covariance function is given by Eq. (8); the demonstration of this equation can be found in Mantoglou and Wilson (Mantoglou and Wilson 1982) and Matheron (Matheron 1973).

$$C_1(r) = \frac{d}{dx}[rC_3(r)] \qquad (8)$$

Where $C_1(r)$ is the unidimensional covariance function, and $C_3(r)$ is the three-dimensional covariance function. $C_3(r)$ is computed using data from three-dimensional data representing a natural rough rock surface. In this project, the spherical covariance function is used to fit the variogram, that is to say $C_3(r)$ computed according to Eq. (6). Thus, a unidimensional equivalent of a spherical covariance function can be determined using Eq. (9).

$$C_{1D}(h) = \begin{cases} b\left(1 - 3\frac{|r|}{a} + 2\frac{r^3}{a^3}\right) & for\ 0 \le |h| \le a \\ 0 & for\ |h| > a \end{cases} \qquad (9)$$

Furthermore, the implementation of the simulation of the random field using the turning bands used in this research is based on the Matlab computer program presented in Emery and Lantuéjoul (Emery and Lantuéjoul 2006).

2.4 Results of the synthetic rough rock surface generator

As stated in section 2.1, the random field simulation to generate synthetic rough rock surfaces proceeds in six steps (Fig. 1).

The first step involved collecting the roughness information of natural rough rock surfaces. Granite blocks with natural rough surfaces were scanned using a laser-based scanner. The distance between the scanned points is 0.025 mm, and the vertical resolution of the scanner is 0.05 mm. The selection of this point density is based on the discussion of the effect of point spacing in the roughness characterization and the peak shear strength estimation (B. S.A. Tatone, Grasselli, and Cottrell 2010), and the vertical resolution is adequate for the scale of this study. From the scanning, localized fields of heights of asperities were obtained. The collected data is then interpolated using Matlab functions to get fields of asperities with a regular grid. This regularization of the grid makes the computation of the roughness and the variograms easy. Fig. 4 illustrates how this step is applied to the present study.

The second step involved applying the quantile-to-quantile normal score transformation to obtain normal distributions of the fields of heights of asperities. Fig. 2 illustrates how this step is applied to the present study.

The variogram analysis is carried out in step three. This analysis determines the covariance function parameters used as inputs of the random field simulation. Fig. 3 illustrates the result of a variogram analysis applied to the present study.

In step four, the random field simulation using the turning bands method is carried out. Fig. 5 illustrates the theoretical variogram from which the simulation inputs were drawn, the variograms of the simulated fields, and the average of the variograms of the simulated fields.

In step five, the back-transformation is carried out to transform the synthetic surfaces obtained from normal distribution to the original distribution of the field used as input. Fig. 6 illustrates two synthetic rough rock surfaces generated.

The last step is the computation of roughness parameters of the synthetic rough rock surfaces to select synthetic rough rock surfaces with specific roughness values. The roughness characterization is performed using the Grasselli roughness parameter $\theta^*_{max}/(C+1)$ (Bryan S. A. Tatone and Grasselli 2009). Fig. 7 shows the 334 synthetic rough rock surfaces selected for finite element simulations of direct shear tests of concrete-rock interfaces to study the effect of roughness on the shear behavior of interfaces. The roughness of the 334 synthetic rough rock surfaces generated in this study (Fig. 7) varies between 6° and 24°($\theta^*_{max}/(C+1)$).

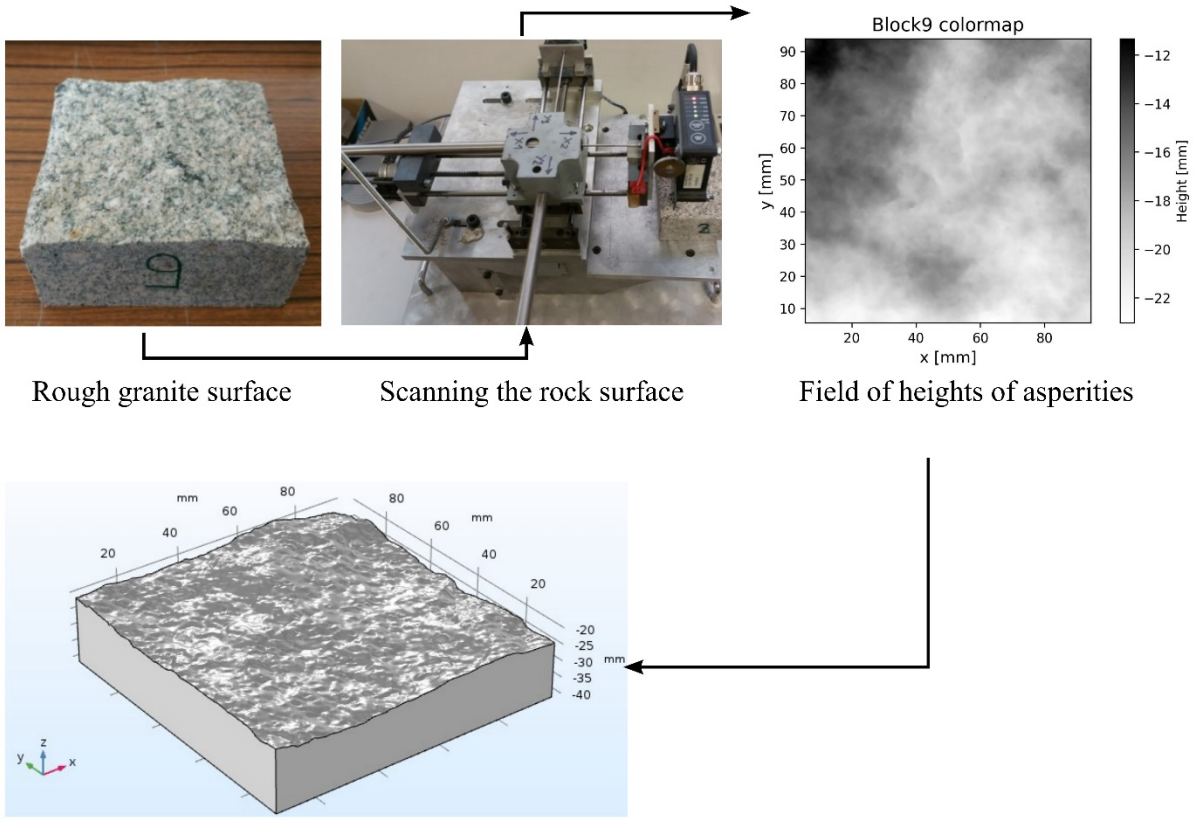

Fig. 4 Scanning rough rock surface (step 1 of the synthetic rock surface generation process)

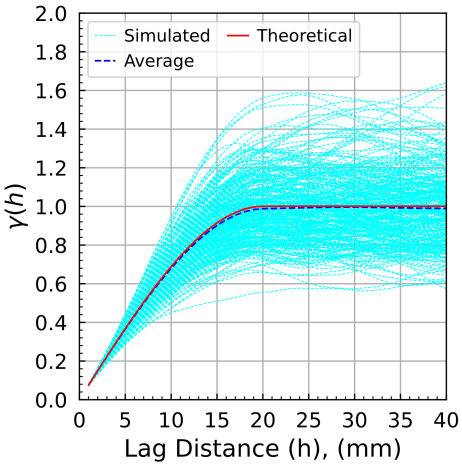

253 **Fig. 5** Variograms of simulated rough rock surfaces (step 4 of the synthetic rock surface generation process)
254
255

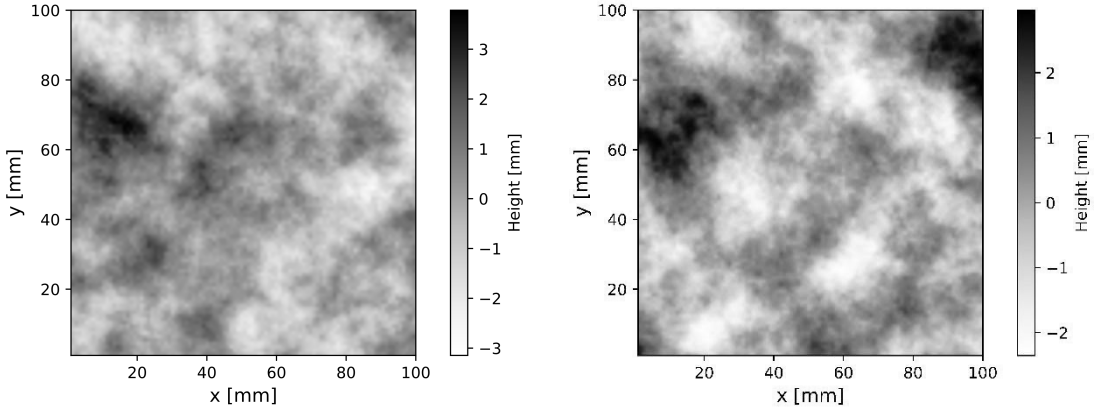

256 **Fig. 6** Synthetic rough rock surfaces generated; **(a)** sample 1 and **(b)** sample 2 (step 5 of the synthetic rock surface
257 generation process)
258
259

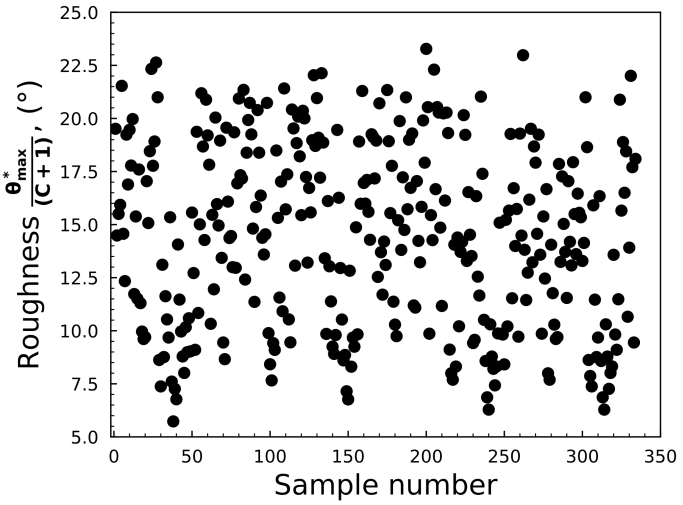

Fig. 7 Roughness of the synthetic rough rock surfaces generated; $\theta^*_{max}/(C+1)$ (step 6 of the synthetic rock surface generation process)

3. Finite elements simulations

3.1 The rationale of the numerical simulation

The finite element simulations performed in this research are based on the experimental and numerical study of the shear resistance of concrete-rock interfaces in the condition of low normal stress presented in Badika et al.(Badika et al. 2022). These authors reported a series of direct shear tests of smooth concrete-granite, bush-hammered concrete-granite, and natural rough concrete-granite interfaces using three levels of normal stress: 0.5, 1.0, and 1.5 MPa. These tests were performed under constant normal loading (CNL). Details regarding the direct shear test machine used are presented in Boulon (Boulon 1995). A complete presentation of the mechanical characterization of concrete and granite as intact materials is presented in the literature (Mouzannar 2016; El Merabi 2018). The analysis of this experimental study led to three significant observations. The formation of strong concrete-rock bonds depends on the micro-roughness of the granite surfaces. The macro-roughness of the granite surfaces influences the shear behavior of concrete-rock interfaces through surfaces interlocking. Depending on the normal stress, two failure modes are possible: the first failure mode (with a normal stress of 0.5 MPa) proceeds along the interface with no significant damage in either concrete or rock, and the second failure mode (with a normal stress of 1.0 and 1.5 MPa) proceeds mainly along the interface but also shears the tips of concrete. Overall, this experimental study shows that the shear behavior of concrete-rock interfaces happens at the interface and is driven by the micro-roughness and macro-roughness of the rock surface.

Since failure is observed mainly at the interface, the choice was made to concentrate on the non-linearities at the interface. With these outcomes, the cohesive frictional model proposed by Tian et al. (Tian et al. 2015) was used to simulate the shear behavior of concrete-rock interfaces. In this model, the behavior law simulates the micro-roughness and, therefore, the concrete-rock bonds. The calibrated cohesive-frictional model presented by Badika et al. (Badika et al. 2022) is used in the present research. In this model, the local evolution of the shear stress is composed of three successive phases. The first phase is linear elastic and mainly driven by the concrete-rock bonds. The second phase is characterized by a progressive failure of the bonds (using a damage constitutive law) and progressive friction mobilization. The third phase is driven by friction. The equations of the cohesive-frictional model are detailed in (Badika et al. 2022). The calibration of the parameters of this model was performed using the results of direct shear tests of bush-hammered concrete-granite interfaces. The influence of the concrete strength in the second failure mode leads to a different value of the parameters used in the interface constitutive law. This is why there are two sets of parameters for the calibrated model, presented in Table 1. The explicit representation of the rough rock surface

introduces the influence of macro-roughness. Apart from the interface, concrete and rock are considered linear elastic materials, with properties displayed in Table 2.

Table 1 Parameters of the model (Badika et al. 2022)

Cohesive frictional model	Parameters	First failure mode (0.5 MPa)	Second failure mode (1.0 - 1.5MPa)	Unit
Cohesive part	Normal stiffness	15	15	GPa/m
	Shear stiffness	7.5	4.5	GPa/m
	Normal strength	1	1.4	MPa
	Shear strength	1.2	1.6	MPa
	Shear displacement	0.9	2.25	mm
	Rate of damage evolution	4	4	-
Frictional part	friction coefficient	0.7	0.65	-

3.2 Preparation of the simulation

The point clouds representing the field of heights of asperities composing the rough rock surfaces were generated using random field simulations (refer to section 2). Then, the point clouds generated were converted into surfaces through interpolation. Each surface obtained was used to create a 3D solid part using Comsol, which was later imported into Abaqus. With this imported 3D solid part and the merge and cut tool in Abaqus, two perfectly matched parts were generated to represent the concrete and granite blocks for the simulation of the direct shear test.

The mesh size was defined such that the macro-roughness of the rock surface is faithfully represented. The average mesh size of 4 mm was used. The fully integrated eight-node brick element (C3D8) was selected for the simulation.

After meshing, there is a possibility of initial overclosure. The initial overclosure is when the mesh generation modifies slightly the contacting surface of the two bodies such that they might have a few nodes that intrude on each other. To deal with this issue, strain-free adjustments of the intruding nodes are conducted. These adjustments modify the position of the nodes at the interfaces to ensure that concrete and granite blocks are not intruding on each other. This procedure has no significant consequence in representing macro-roughness but is necessary for the convergence of the solution.

The boundary conditions are set to reproduce experimental conditions, see Fig. 8. The normal stress is applied as the pressure in the top part of the half shear box (y direction). The shear boxes apply the shear loading as displacement (x-direction), and no motion is allowed in the third direction (z-direction).

The properties of the concrete, rock, and encasing steel box used in the simulation are presented in Table 2.

It should be noted that only two levels of normal stress are considered: 0.5 and 1.5 MPa, and the nominal area of the interface is 100x100 mm^2.

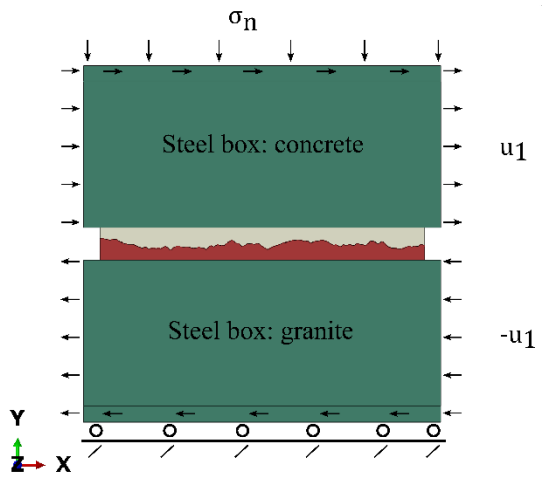

Fig. 8 Boundary conditions

Table 2 Properties of concrete, granite, and steel

Material	Density (kg/m3)	Young's modulus (Gpa)	Poison's ratio
Concrete	2370	38	0.20
Granite	2608	60	0.25
Steel	8000	193	0.29

3.3 Results of the finite element simulations

Fig. 9 presents a selection of the results of the virtual direct shear tests of synthetic rough rock surfaces for each failure mode mentioned in section 3.1. The shear evolution obtained comprises a pre-peak phase followed by a post-peak phase and is completed by a residual phase. The succession of these phases is the reproduction of the main stages encountered in experimental results of the direct shear tests of concrete-rock interfaces (Saiang, Malmgren, and Nordlund 2005; Moradian, Ballivy, and Rivard 2012; Moradian et al. 2010). From both figures, it is clear that the roughness of the interfaces influences the peak shear strength. Furthermore, these figures also show that the peak shear strength depends on the normal stress. It should be pointed out that all the 334 interfaces virtually tested have different roughness values.

Fig. 10 shows the peak shear strength of the interface in terms of roughness. The correlation coefficients between the peak shear strength and the $\theta^*_{max}/(C+1)$ are 0.88 and 0.85 for the simulations performed with 0.5 and 1.5 MPa, respectively. These results show that the peak shear strength maintains a strong correlation with the roughness of the interface when the normal stress is below 1.5 MPa.

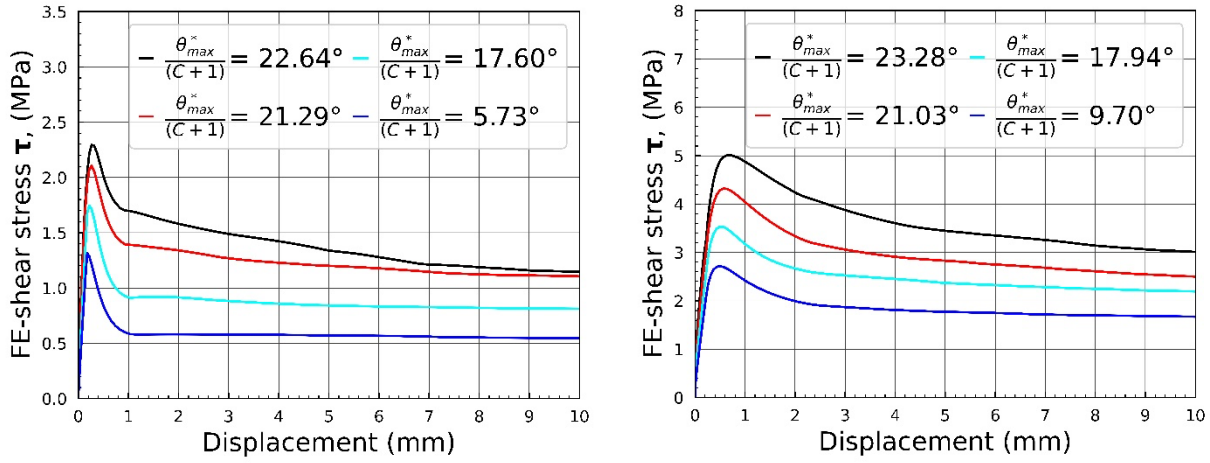

(a) **(b)**

Fig. 9 Selected results of the finite element simulations: **(a)** first failure mode (0.5 MPa) and **(b)** second failure mode (1.5 MPa)

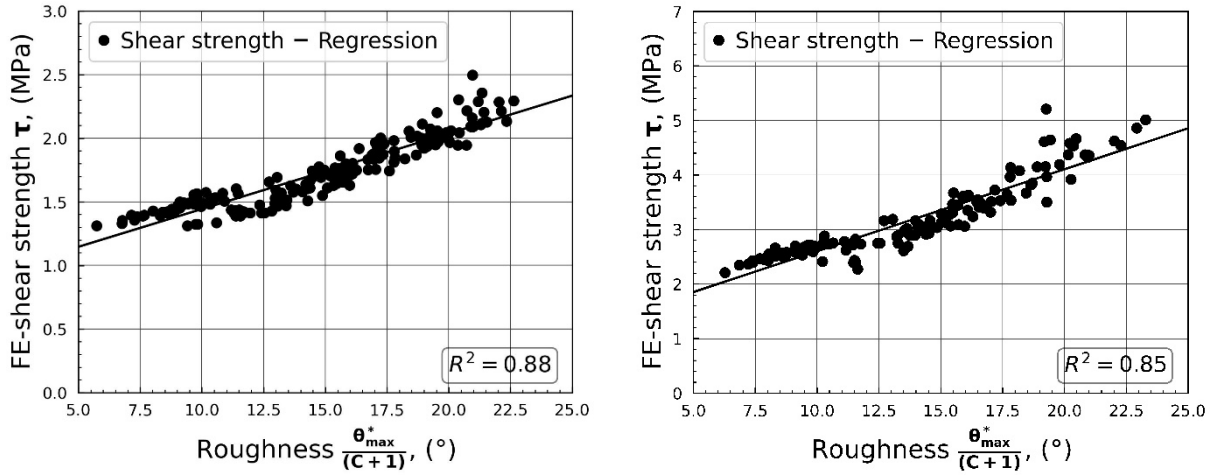

$$\tau_p = 0.0594\left(\frac{\theta^*_{max}}{C+1}\right) + 0.8493$$

$$\tau_p = 0.1501\left(\frac{\theta^*_{max}}{C+1}\right) + 1.1036$$

(a) **(b)**

Fig. 10 Peak shear strength in terms of roughness; **(a)** normal stress 0.5 MPa and **(b)** normal stress 1.5 MPa

Fig. 10 also shows that interfaces with the same or very similar roughness values do not always result in the same peak shear strength. This observation indicates that the relationship between the roughness and the peak shear strength is not always one-to-one. The reason for the non-unicity roughness-peak shear strength could be related to the global aspect of the roughness parameter. In fact, $\theta^*_{max}/(C+1)$ evaluates the global roughness of a rock surface and does not focus on the local influence of roughness. Rullière et al. (Rullière et al. 2020) also reported a similar observation. This observation indicates that the local aspect of roughness explicitly considered in the finite element simulations can significantly influence the shear behavior of interfaces.

Overall, the results of the finite element simulations constitute an extensive database of shear evolutions in terms of the roughness of interfaces tested. With this database, two approaches are used to define a failure criterion for concrete-

rock interfaces under low normal loading. The first failure criterion proposed is an analytical relationship, while the second is a function based on neural network modeling.

4. Peak shear strength criterion for rough concrete-rock interface

4.1 Development of a new failure criterion for rough concrete-rock interfaces

The proposed peak shear strength criterion for concrete-rock interfaces under the CNL condition is based on the peak shear strength criterion for rock joints subjected to the CNL condition developed by Grasselli and Egger (Grasselli and Egger 2003); see Eq. 10.

$$\tau_p = \sigma_n \tan\left[\phi_b + \left(\frac{\theta^*_{max}}{C}\right)^{1.8}\right]\left[1 + e^{-\left(\frac{\theta^*_{max}}{9A_0C}\right)\left(\frac{\sigma_n}{\sigma_t}\right)}\right] \quad (10)$$

where τ_p is the peak shear strength. σ_n is the normal stress. ϕ_b is the basic friction angle. θ^*_{max}/C is the roughness parameter. A_0 is the maximum contact area during shear. σ_t is the tensile strength of the rock.

The contribution of roughness in this shear strength criterion can be replaced by the updated expression of roughness presented by Tatone and Grasselli (Bryan S. A. Tatone and Grasselli 2009); this yields Eq. 11.

$$\tau_p = \sigma_n \tan\left[\phi_b + \left(\frac{\theta^*_{max}}{C+1}\right)^{1.8}\right]\left[1 + e^{-\left(\frac{\theta^*_{max}}{C+1}\right)\left(\frac{\sigma_n}{\sigma_t}\right)}\right] \quad (11)$$

where $\theta^*_{max}/(C+1)$ is the roughness parameter.

For the case of concrete-rock interfaces under low normal stress, the failure criterion depends on both friction and cohesion. The cohesion is crucial in the case of low normal stress because its contribution to the shear resistance of the interface is significant and cannot be ignored. Therefore, the cohesion of the concrete-rock interface is included in Eq. 11, generating Eq. 12. Eq. 12 is a failure criterion for concrete-rock interfaces.

$$\tau_p = \sigma_n \tan\left[\phi_b + \left(\frac{\theta^*_{max}}{C+1}\right)^{1.8}\right]\left[1 + e^{-\left(\frac{\theta^*_{max}}{C+1}\right)\left(\frac{\sigma_n}{\sigma_t}\right)}\right] + c \quad (12)$$

For the synthetic rough rock surfaces generated, $\theta^*_{max}/(C+1)$ varies between 6º and 24º. The normal stress in the finite element simulations is 0.5 and 1.5 MPa. If one assumes the tensile strength is equivalent to 1 MPa, $e^{-(\theta^*_{max}/(C+1))(\sigma_n/\sigma_t)}$ varies between 0 and 0.08 and can be neglected in Eq. 12. This generates Eq. 13

$$\tau_p = \sigma_n \tan\left[\phi_b + \left(\frac{\theta^*_{max}}{C+1}\right)^{1.8}\right] + c \quad (13)$$

Eq. 13 represents the proposed peak shear strength criterion for rough concrete-rock interfaces in the case of low normal stress.

4.2 Validation of the new failure criterion for rough concrete-rock interfaces

The shear responses obtained in the finite element simulations of direct shear tests using synthetic rough rock surfaces are used here to assess the capability of the proposed failure criterion to estimate the peak shear strength of the concrete-rock interface.

For each synthetic rough rock surface virtually tested, its normal stress σ_n, basic friction angle ϕ_b (30°), roughness parameter $\theta^*_{max}/(C+1)$ and cohesion are used as input of Eq. 13 to obtain the estimated peak shear strength τ_p.

The cohesion of concrete-rock interfaces depends on the normal stress, the failure modes, and the strength of the concrete-rock bonds. The cohesion of the concrete-rock interface is usually determined indirectly using the fitting of the Mohr-Coulomb failure envelope computed, for example, using the results of direct shear tests. For the cohesion defined using this approach to be valid, all the shear test results must be within a range of normal stress representing the same failure mode.

In the specific case of concrete-granite interfaces under low normal stress, as considered in this research, the cohesion is determined using the results of the direct shear tests of bush-hammered concrete-granite interfaces. The fitting includes the shear strength of interfaces under three normal stress levels: 0.5 MPa, 1.0 MPa, and 1.5 MPa. Within this interval of normal stress, two failure modes were identified (El Merabi 2018). The cohesion defined using the data of the two failure modes is expected to be underestimated in the case of shear strength under 0.5 MPa of normal stress and overestimated in the case of normal stress between 1 and 1.5 MPa. The computation of the failure envelope yields a cohesion of 0.83 MPa. Updating this value for the two failure modes produces a 0.99 and 0.69 MPa cohesion.

The peak shear strength of all the synthetic rough rock surfaces simulated using Eq. 13 is presented in Fig. 11 (a) for the first failure mode and in Fig. 11 (b) for the second failure mode. The correlation coefficient between the estimated and the simulated peak shear strength is 0.91 for the first failure mode and 0.90 for the second failure mode. These coefficients show that the proposed peak shear strength criterion can estimate the peak shear strength of concrete-rock interfaces under low normal stress.

The percent error of the estimated peak shear strength compared with the finite element simulated peak shear strength is presented in Fig. 12 (a) for the first failure mode and Fig. 12 (b) for the second failure mode. Positive and negative percent errors are used to indicate underestimation and overestimation. Fig. 12 (a) and Fig. 12 (b) show that the percent error of the model is within fifteen percent for the first failure mode and twenty percent for the second failure mode. Furthermore, the shape of these two figures is associated with the inclusion of the roughness value inside a tangential operation in the proposed failure criterion (Eq. 13). It must be stressed that the two failure modes were defined for concrete-granite interfaces where shear failure mostly occurs along the interfaces for normal stress below 1.5 MPa.

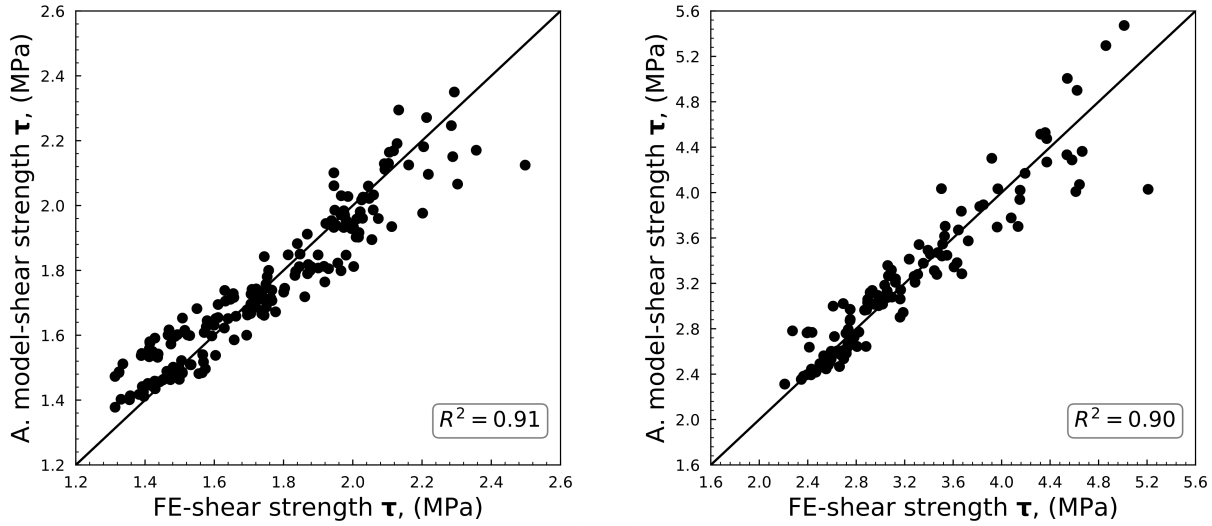

(a) **(b)**

Fig. 11 Peak shear strength estimated using the analytical model in terms of numerically obtained peak shear strength: **(a)** first failure mode (0.5 MPa) and **(b)** second failure (1.5 MPa)

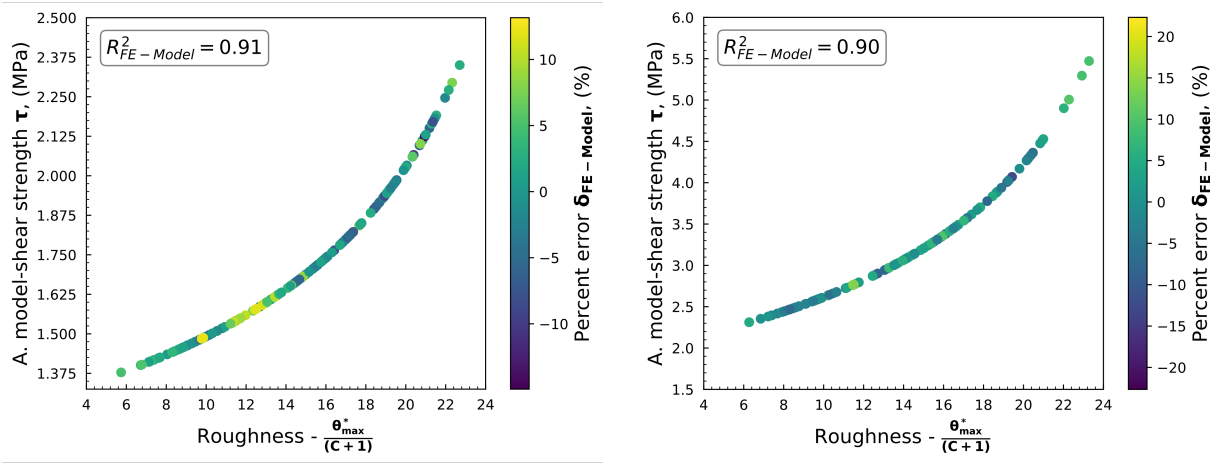

(a) **(b)**

Fig. 12 Error of the estimated peak shear strength in terms of the simulated peak shear strength; **(a)** first failure mode (0.5 MPa) and **(b)** second failure mode (1.5 MPa)

From Fig. 12, it is clear that Eq. 13 supposes that the relationship between the roughness and the peak shear strength is one-to-one. Indeed, the local roughness seems to influence the shear resistance of the interface significantly. To address the limitation of the bijective nature of the relationship roughness-peak shear strength as assumed in Eq. 13 and to take advantage of complex statistical aspects of the database of shear evolutions obtained by finite element simulation of direct shear tests of synthetic rough rock surfaces, a neural network modeling is investigated as a complementary alternative to define a failure criterion for concrete-rock interfaces.

5. Peak shear strength of concrete-rock interfaces using neural network modeling

The neural network model is set as a function f_{NN} that predicts the peak shear strength (τ_{NN}) of a concrete-rock interface using the normal stress (σ_n), the basic friction angle (Φ_b) and the roughness parameter $\theta^*_{max}/(C+1)$, see

Eq. 14. This function is very similar to the peak shear strength criterion presented in section 4; they both use the same input parameters and intend to estimate the same output parameter.

$$f_{NN} : \left\{\sigma_n, \Phi_b, \frac{\theta^*_{max}}{(C+1)}\right\} \rightarrow \{\tau_{NN}\} \qquad (14)$$

5.1 Neural network modeling

5.1.1 Dataset

The data for the neural network modeling is composed of 334 entries (rows). Each entry is composed of four values (columns). The first value is the normal stress σ_n used in the simulation. The second value is the basic friction angle Φ_b. The third value is the roughness $\theta^*_{max}/(C+1)$, which represents the roughness of a simulated synthetic rough rock surface. The last value is the peak shear strength (τ_{FE}), the highest shear stress recorded in the shear response obtained via finite element simulation of direct shear test. The normal stress σ_n, the basic friction angle Φ_b, and the roughness $\theta^*_{max}/(C+1)$ are the input data, while the peak shear strength (τ_{FE}) is the expected output data. The entire data contains 1336 data points.

The columns of the data are feature-wise normalized to make the training of the neural network easier. The feature-wise normalization consists of subtracting each value from the mean of the column and dividing by the standard deviation of the column.

The data is randomly separated into two sets to train the model: the training and the validation datasets. The training dataset is used to train neural network models. The validation dataset is used to test the performance of trained neural network models.

The proportion of the split is 50% of the data is the training dataset, and 50% is the validation dataset. The division attempts to maintain the distribution of the data. Fig. 13 illustrates this data separation.

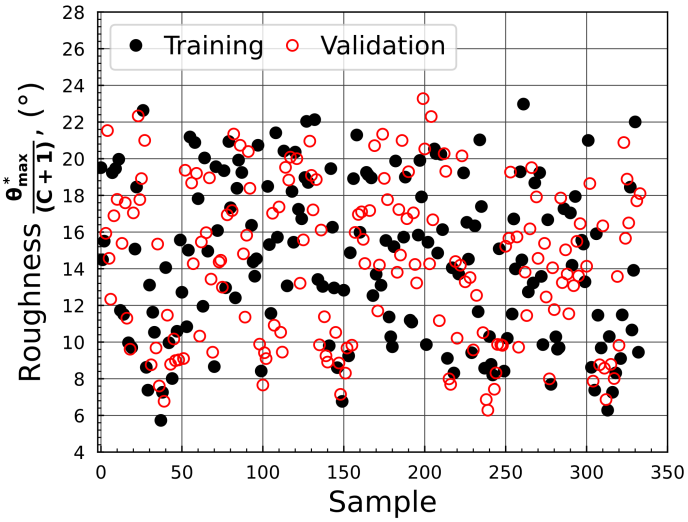

Fig. 13 Training and validation datasets

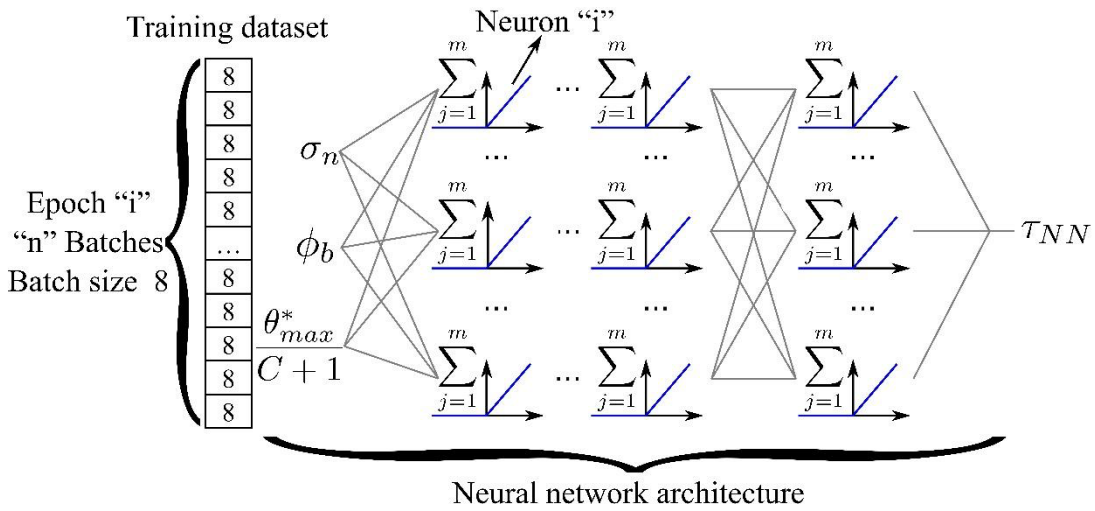

Fig. 14 Basic concepts of ANN: Neural network architecture, neurons, training dataset, batches, and batch size and epoch

5.1.2 Training of the neural network model

After the preparation of the datasets, a brief insight into how the neural network is trained to receive as input the normal stress σ_n, the basic friction angle Φ_b, and the roughness $\theta^*_{max}/(C+1)$ and to produce as output the peak shear strength τ_{NN} is presented.

A typical neural network architecture comprises an input, hidden, and output layer. The input layer is fed with the input data, the hidden layers transform the input data into valuable statistical representations, and the output layer provides the prediction or the output data. Fig. 14 presents an illustration of the architecture of a neural network for the estimation of the peak shear strength of concrete-rock interfaces τ_{NN} using as inputs the normal stress σ_n, the basic friction angle Φ_b, and the roughness $\theta^*_{max}/(C+1)$.

Layers of neural networks are composed of one or multiple neurons (Fig. 14). The neurons carry out the transformations that layers apply to the input data (σ_n, Φ_b, $\theta^*_{max}/(C+1)$). A neuron computes the weighted average of the incoming inputs, uses an activation function, and returns an output value. The weights constitute the parameters of the neural network model. In most cases, including this study, the activation function adds non-linearity to the inputs to produce an output.

A detailed representation of a neuron is shown in Fig. 15. In this figure, if the neurons belong to the first layer after the input layer, X_I is equivalent to (σ_n, Φ_b, $\theta^*_{max}/(C+1)$). If the neurons belong to the output layer, Y is equivalent to the estimated peak shear strength τ_{NN}. Otherwise, X_i are transformations resulting from the preceding layer, and Y is a transformation passed on to the next layer.

The training of the neural network is the attempt to find the appropriate values for the weights w_i of the neurons (Fig. 15) to be able to associate inputs (σ_n, Φ_b, $\theta^*_{max}/(C+1)$). to output (τ_{NN})

During one pass of the training of a neural network, the input layer receives one or multiple entries (σ_n, Φ_b, $\theta^*_{max}/(C+1)$). from the training dataset. The hidden layers use operations performed by the neurons to transform the input data into more valuable representations. The output layers use the generated representations to predict the output values (τ_{NN}). The predicted values are then compared to the expected values (τ_{FE}) using the loss function; this generates the loss score, which is then used by the optimizer to modify the weights w_i using a back-propagation algorithm. Notably, the parameters of the neural network model are randomly initialized before the first pass.

It should be noted that the batch size is the number of entries of the training dataset fed to the neural network during a single pass. A batch size of 8 is used in the training of the ANN in Fig. 14. An epoch is an iteration consisting of one or multiple passes during the training of the neural network model completed when all the training dataset has been used to find the best parameters (weights, w_i) of the neural network model (a single epoch "i" is presented in Fig. 14).

It is important to note that the ANN used in this study can be correctly classified as a Deep neural network (DNN). However, as considered in this study, the problem of predicting or estimating a value or a series of values constitutes the regression problem. Since the DNN developed has been learned by exposure to correct mapping (input data – known output), it can be classified as a supervised learning algorithm.

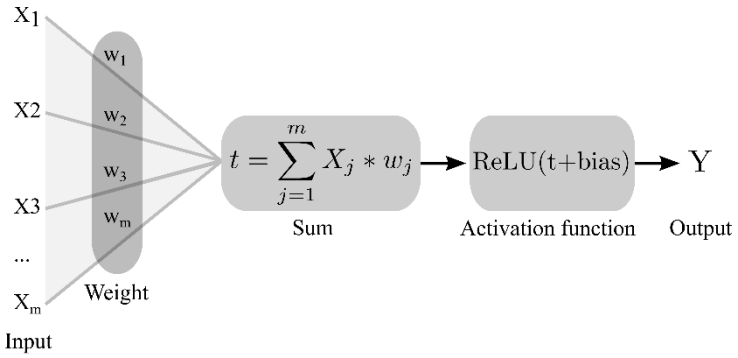

Fig. 15 Neuron of a neural network

During training, after each epoch, the performance of the updated neural network model is assessed using the validation dataset. The report of the performance of successive neural network models on the training and validation dataset is called the learning curve. From the learning curve, the best neural network model can be selected.

During the training of the model to estimate the peak shear strength of concrete-rock interfaces τ_{NN}, different architectures composed of different numbers of layers, different numbers of neurons per layer, and different batch sizes were assessed. This assessment, called hyperparameters analysis, is important to determine the best architecture. The report of the hyperparameters analysis is presented in section 5.2.

All the architectures of the neural networks analyzed start with an input layer that receives the input parameters of the model; this means the normal stress σ_n, the basic friction angle Φ_b and the roughness $\theta^*_{max}/(C+1)$. The input layers are followed by hidden layers, each with a defined number of neurons. The result of each neuron is obtained using the activation function ReLU (rectified linear unit). This function screens out all the negative values. After the data contained in each batch has been estimated by the neural network as part of a single step of an epoch, it is important to assess the quality of the performance of the neural network. This assessment is carried out using a loss function. The mean squared error (MSE) presented in Eq. 15 is the loss function used in this study. The optimizer uses the outcome of the loss function to modify the weights of the neural network to improve the performance of the model in the next step.

$$\mathrm{MSE} = \frac{1}{\mathrm{n}}\sum_{\mathrm{i}=1}^{\mathrm{n}}(\tau_{\mathrm{NN}} - \tau_{\mathrm{FE}})^2 \qquad (15)$$

Where n is the number of data, τ_{NN} is the peak shear strength predicted by the neural network, and τ_{FE} is the peak shear strength obtained by finite element simulation, τ_{FE} are part of the datasets.

The optimizer used is ADAM (Adaptive Momentum Estimation) (Kingma and Ba 2015). The mean absolute error (MAE) is used as a metric to assess the performance of the neural network model trained to estimate the peak shear strength of the concrete-rock interface after each epoch (see Eq. 16).

$$\mathrm{MAE} = \frac{1}{\mathrm{n}}\sum_{\mathrm{i}=1}^{\mathrm{n}} |\tau_{\mathrm{NN}} - \tau_{\mathrm{FE}}| \qquad (16)$$

The output layer is the last layer that predicts the peak shear strength τ_{NN}.

Furthermore, all the codes used were developed in Keras. Keras is a deep-learning framework for Python where neural network models can be set, trained, and assessed (Chollet 2021). TensorFlow backend engine handled tensor operations and differentiation (Abadi et al. 2016).

5.2 Results of the neural network modeling

This section comprises two parts: the hyperparameters analysis and the presentation of the results of the neural network model focusing on estimating the peak shear strength.

5.2.1 Hyperparameters analysis

The hyperparameter analysis is carried out to define the best neural network architecture for the estimation of the peak shear strength τ_{NN} of concrete-rock interfaces. The hyperparameters considered in this analysis are the number of layers per neural network, the number of neurons per layer, and the batch size. For each hyperparameter, neural network models with different architectures are assessed regarding the quality of the estimation of the peak shear strength τ_{NN} when tested using the validation dataset (σ_n, Φ_b, $\theta^*_{max}/(C+1)$, τ_{FE}). This assessment uses the MAE (Eq. 16) as a performance indicator.

To consider the oscillations of the performance of models when the training process is repeated, for each neural network model considered, the training was repeated five times, and only the average performance was reported.

Fig. 16 (a) shows the influence of the number of layers on the performance of the neural network models. Each point in this figure is equivalent to the best performance obtained after completing training a model. The performance of the models increases with the increase of the number of layers m when m is between 2 and 6. It remains constant or tends to decrease afterward. Therefore, the number of layers of 6 was adopted for subsequent analysis.

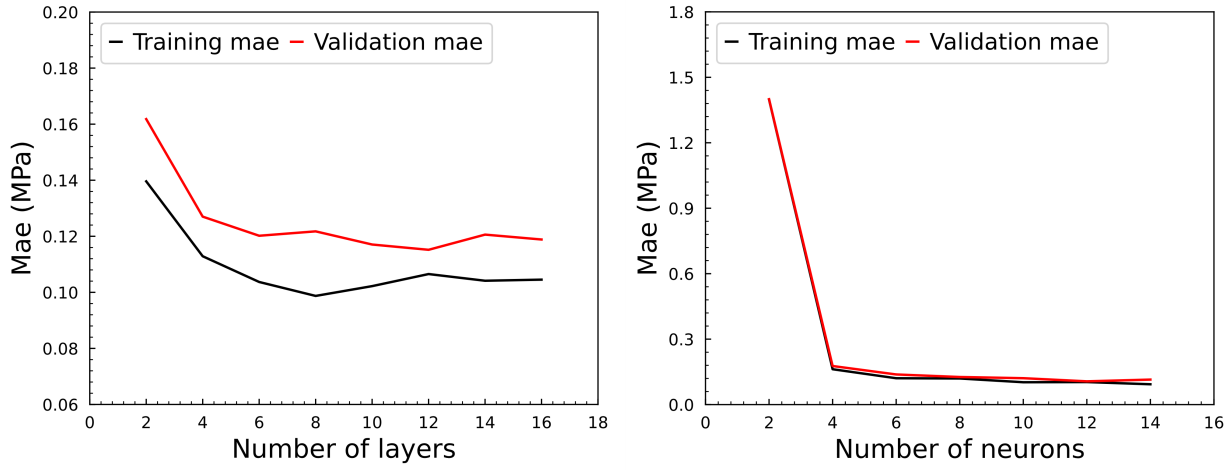

(a) **(b)**

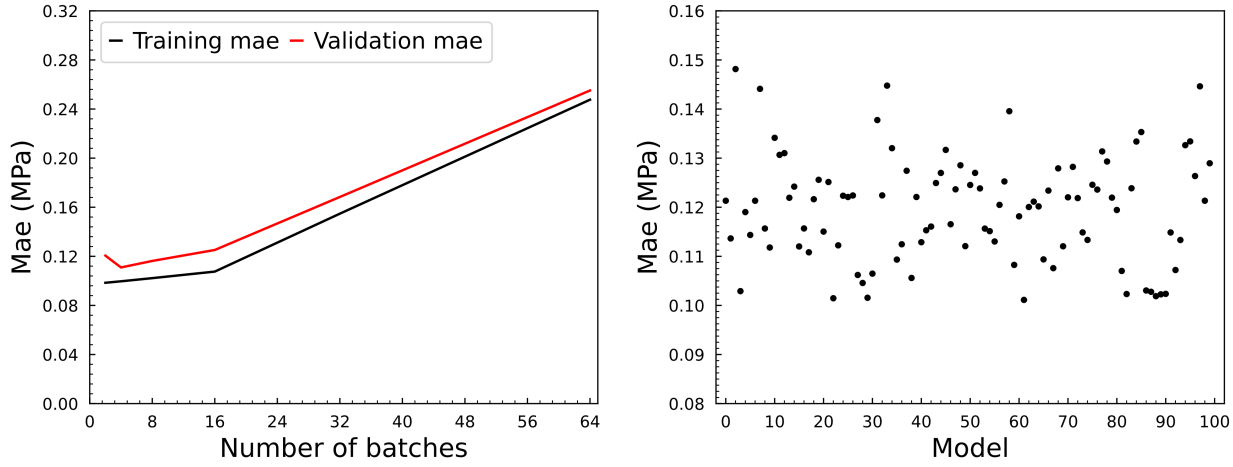

(c) **(d)**

Fig. 16 Results of hyperparameter analysis: **(a)** influence of the number of layers, **(b)** influence of the number of neurons, **(c)** influence of the batch size, and **(d)** variation of the ANN model

Fig. 16 (b) shows the influence of the number of neurons per layer on the performance of the neural network. The performance of the models increases with the increase of the number of neurons per layer n when n is below 6. Beyond this limit, the performance of the model becomes insensitive to the rise of n. A number of neurons of 10 is adopted for subsequent analysis.

The last hyperparameter to consider is the batch size. Batch sizes varying from 2 to 64 were investigated. From Fig. 16 (c), it is clear that increasing the batch size reduces the performance of the neural network. Therefore, the batch size of 8 was adopted.

From this analysis, the architecture of the most suitable model for estimating the peak shear strength of concrete-rock interfaces contains one input layer, six hidden layers, each composed of ten neurons, and one output layer that predicts the peak shear strength τ_{NN}.

The training of the model to predict the shear strength τ_{NN} using the defined neural network architecture is repeated 100 times to assess the variation in the performance of the model. The results of this analysis are presented in Fig. 16 (d) and show that the variation in the performance of the model is not significant with an MAE (Eq. 16) between 0.10 and 0.15 MPa.

5.2.2 Performance of the neural network model

The history of the performance of the neural network models during training is presented in Fig. 17. The selected model has a high performance with an MAE of 0.10 MPa in the training data and 0.11 in the validation data.

Fig. 18 (a) presents the estimation of the model when tested with the validation dataset. The correlation between the finite element obtained peak shear strength and the neural network predicted peak shear strength is 0.96 with an MAE of 0.11. Fig. 18 (b) shows the error of the neural network model prediction on the validation dataset compared to the finite element base values. The variation of the prediction error is around 20% and is encouraging.

The two trends observed in Fig. 18 (b) are related to the two normal stresses used in the finite element simulation with normal stress of 0.5 and 1.5 MPa. See section 3.

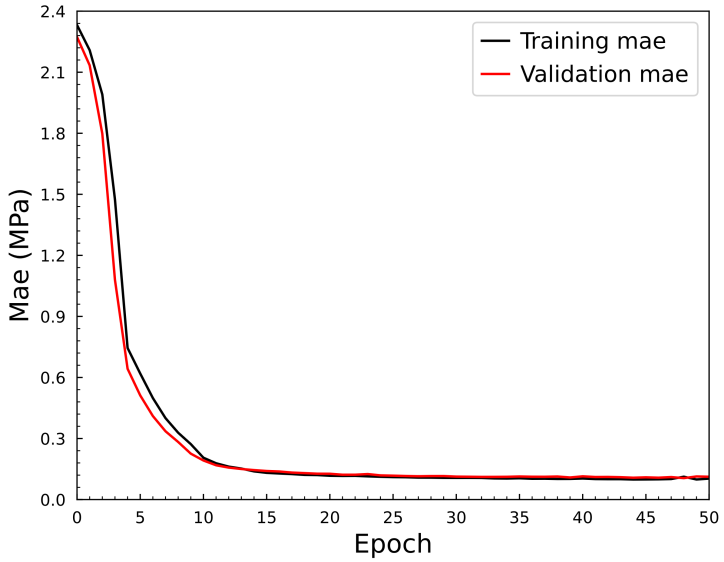

Fig. 17 Performance of the neural network for the estimation of the peak shear strength

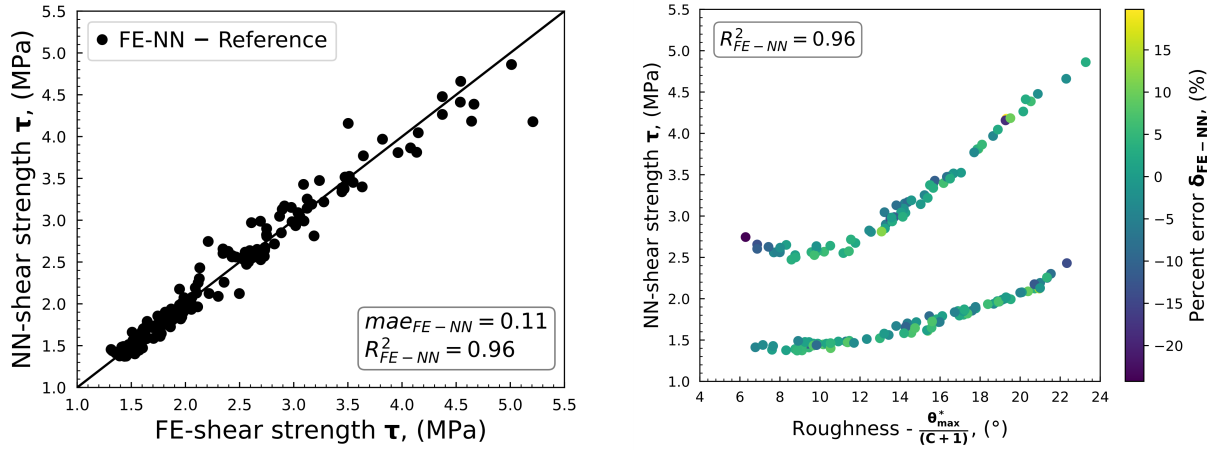

(a) **(b)**

Fig. 18 (a) Finite elements (FE) obtained peak shear strength in terms of neural network (NN) predicted peak shear strength (validation dataset), and **(b)** NN predicted peak shear strength in terms of the roughness and percent error (validation dataset).

6. Assessment of the two failure criteria using experimental data

The performance of the two approaches for estimating the peak shear strength of concrete-rock interfaces is assessed using the experimental results of direct shear tests of rough concrete-granite interfaces submitted to 0.5, 1.0, and 1.5 MPa of normal stress. The results of these tests were briefly discussed in section 3.1 and are fully reported in El Merabi(El Merabi 2018).

However, before applying the two models, the roughness data of the interface tested was interpolated to generate gridded data with a point spacing of 1 mm. This interpolation is important to reach the same point spacing of the synthetic rough rock surfaces used in the finite element simulations and analysis, leading to the two failure criteria. This pre-processing is inspired by the discussion of the influence of point spacing on the computation of roughness and failure criteria, presented by Tatone et al. (B. S.A. Tatone, Grasselli, and Cottrell 2010).

Fig. 19 (a) presents the results of the estimated peak shear strength obtained using the analytical model in terms of the experimentally obtained peak shear strength. The correlation of the estimated in terms of the experimentally obtained peak shear strength is 0.20 for the first failure mode (normal stress of 0.5 MPa) and 0.84 for the second failure mode (normal stress of 1.0 and 1.5 MPa). However, given the low data in each failure mode, it is best to assess the quality of the estimations in terms of the percent error. Fig. 19 (b) shows the percent error of the estimated peak shear strength in terms of the experimentally obtained peak shear strength. This figure shows that the errors are within 25% of the experimental results for most of the estimated peak shear strength.

Fig. 20 (a) shows the variation of the estimated peak shear strength obtained using the neural network model in terms of the experimentally obtained peak shear strength. Notably, only the experimental rough concrete-granite interfaces tested under 0.5 and 1.5 MPa of normal stress are considered in this analysis. This selection is due to the limited variation of data used in the neural network modeling regarding normal stress. Only two levels of normal stress are used: 0.5 and 1.5 MPa. The correlation coefficient between the estimated and the experimentally obtained peak shear strength is 0.96 with an MAE of 0.21 MPa. The good capability of the neural network model is evident when the estimated data is presented in terms of the percentual error, as shown in Fig. 20 (b). This figure shows that the estimations provided are quite close to the experimentally obtained peak shear strength for most of the results.

This assessment shows that the two approaches proposed for estimating the peak shear strength of concrete-rock interfaces can be used for the experimental results. The quality of the estimations is interesting and shows the relevance of the new methodology of investigating the shear behavior of interfaces.

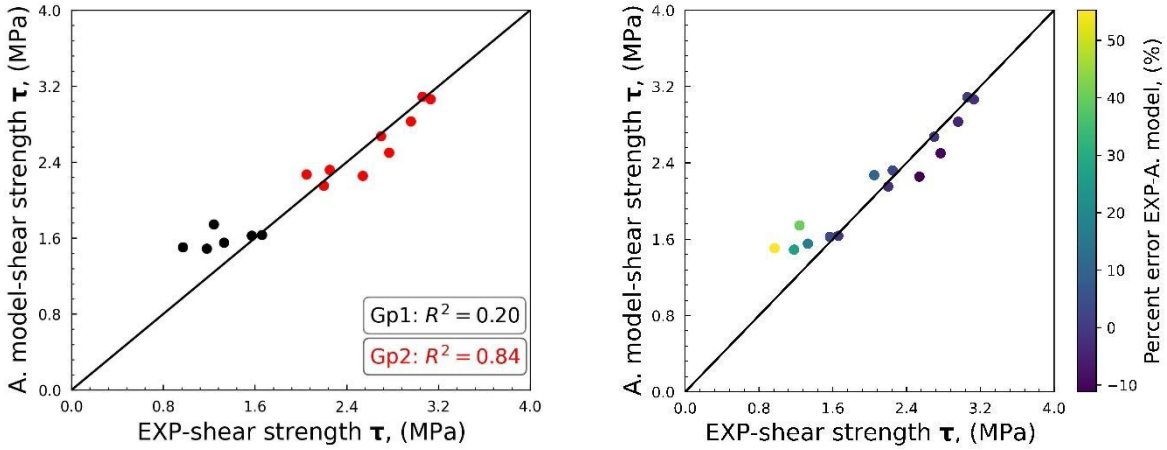

Fig. 19 Assessment of the analytical model: **(a)** Experimental vs estimated peak shear strength and **(b)** Percent error between the Experimental and the estimated peak shear strength

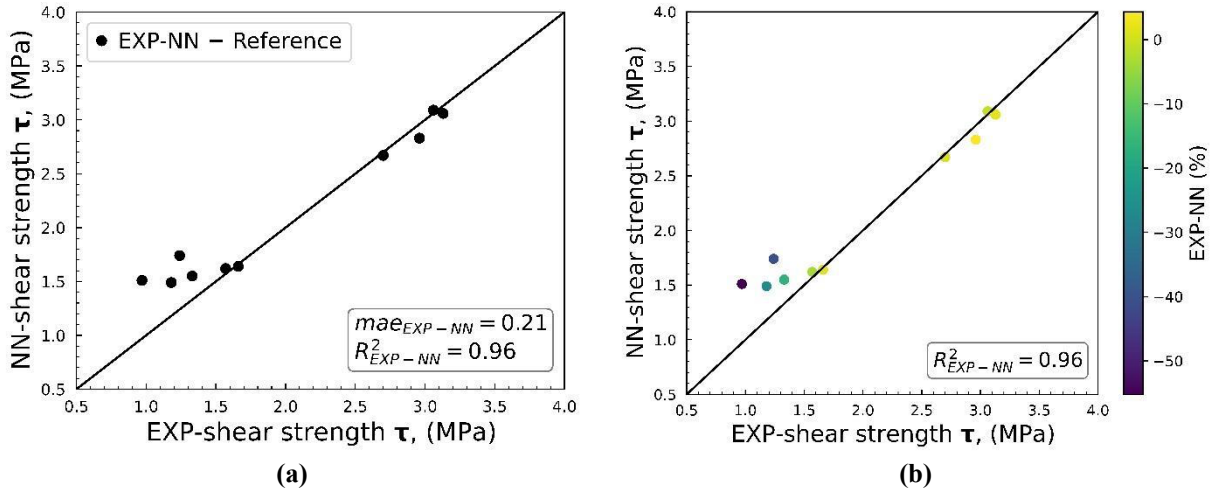

585 **Fig. 20** Assessment of the neural network model: **(a)** Experimental vs estimated peak shear strength and **(b)** Percent
586 error between the Experimental and the estimated peak shear strength
587

588 ## 7. Discussion of the two approaches to estimating the shear strength of concrete-rock
589 interfaces

590 Fig. 21 shows the results of estimating the peak shear strength of concrete-rock interfaces using the analytical and
591 neural network models. The correlation coefficient between the estimated peak shear strength and the finite element
592 simulated peak shear strength is 0.91 and 0.90 for the analytical model considering the two failure modes and 0.96 for
593 the neural network model.

594 From Fig. 21, it is clear that the performance of both the failure criterion and the neural network model is very high
595 (above 0.85), with the neural network results slightly better than those of the analytical model.

596 Fig. 22 shows the error in the estimation of the peak shear strength in terms of the roughness parameter $\theta^*_{max}/(C +$
597 1). This error is approximatively between -20% and 20% for both the analytical and neural network models.

598 Moreover, Fig. 22 also shows that, unlike the analytical model, the neural network model can reproduce the non-
599 bijective relationship between the roughness and the peak shear strength observed in the results of the finite elements
600 simulations (section 3.3).

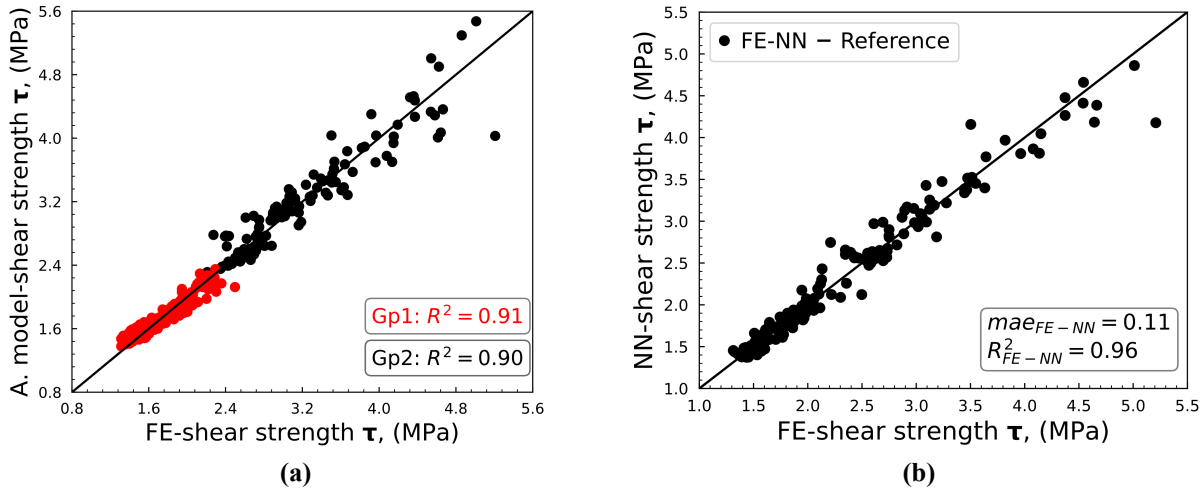

Fig. 21 Estimation of the peak shear strength **(a)** Failure criterion **(b)** Neural network model

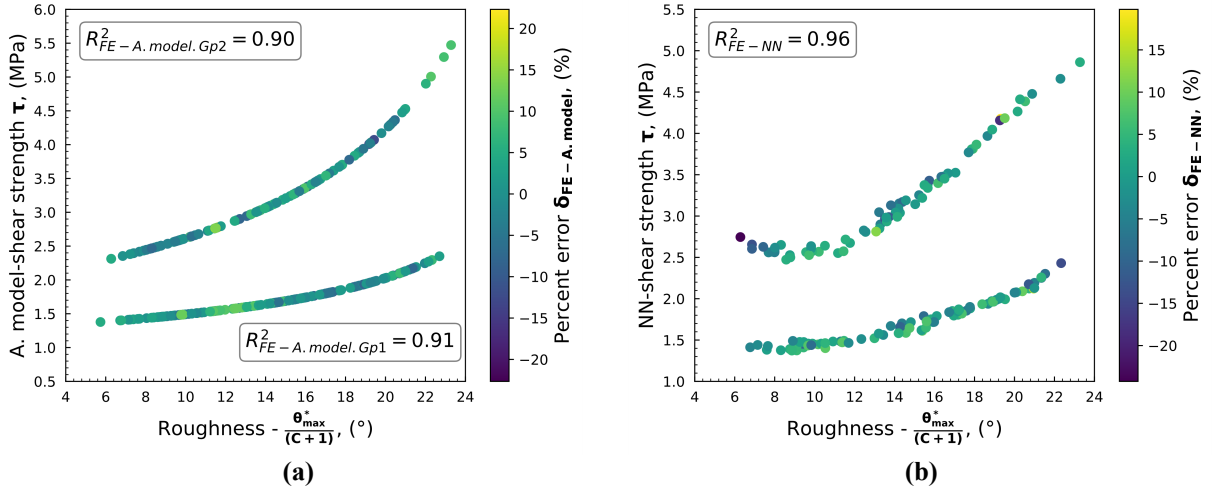

(a) **(b)**

Fig. 22 Error of the estimation of the peak shear strength **(a)** analytical model and **(b)** Neural network model

8. Conclusion

In this paper, a study of the influence of roughness on the shear resistance of concrete-rock interfaces was carried out. This study aimed to reduce the shortcomings of existing failure criteria caused by the challenge of defining a sufficiently diverse and well-distributed database of rough rock surfaces and performing many virtual shear tests.

Random field simulations were performed using the turning bands method to generate an extensive database of rough rock surfaces. The inputs of these simulations were obtained using variogram analysis of natural rough granite surfaces. The results of these simulations led to the selection of 334 synthetic rough rock surfaces with the roughness parameter $\theta^*_{max}/(C+1)$ changing between 6°and 24°. This database of synthetic rough rock surfaces is well distributed and does not present any cluster.

The numerical simulation approach was selected to address the difficulty of performing many tests. The numerical model used is the cohesive-frictional model. With this model, previously validated using experimental results, numerical simulations of direct shear tests of concrete-rock interfaces were performed. The concrete and the rock blocks used in these simulations were created using the generated database of synthetic rough rock surfaces.

The results of the finite elements simulations of direct shear tests were used to generate a database of simulated shear strengths of concrete-rock interfaces. This database is one of the most extensive in the literature in terms of the number and the variation of roughness considered. The results of the numerical simulations are restricted to quasi-static direct shear tests with constant normal loading conditions, and with a relatively low level of normal stress. With the database generated, two approaches were used to propose failure criteria for concrete-rock interfaces. The first approach is a conventional Coulomb-like analytical relationship based on the analytical model proposed by Grasselli and Egger (Grasselli and Egger 2003), and the second approach is a neural network model. Like the analytical model, the neural network model is defined to estimate the peak shear strength using the same parameter used in the proposed analytical model. As a result, the new analytical and new neural network models perform well in estimating the peak shear strength of simulated direct shear tests. These models show promising perspectives in estimating the shear strength of experimental direct shear tests of concrete-rock interfaces.

However, it is worth stating that the neural network slightly outperforms the analytical model regarding the percent error. Moreover, the neural network can reproduce the non-bijective nature of the correlation between roughness and

peak shear strength, which is hypothesized as caused by the limitations of the roughness parameters to capture the contribution of local roughness.

9. Statements and Declarations

Funding The Doctoral School IMEP2, Université Grenoble Alpes, France, funded this research project.

Conflict of interest: No conflict of interest can be declared.

10. Appendix: Neural network-based estimation of the shear response of concrete-rock interfaces

Failure criteria are limited to estimating the peak or the residual shear strength of rock-rock and concrete-rock interfaces. However, estimating the overall shear responses of these interfaces provides more understanding of the shear behavior.

Not many works have focused on estimating the overall shear responses of rock-rock and concrete-rock interfaces. Grasselli and Egger (Grasselli and Egger 2003) proposed a constitutive model to reproduce the evolution of the shear stress of rock-rock interfaces in terms of the shear displacement (Eq. (17)). However, the proposed relationships require prior knowledge of the peak and residual shear strength, which affect their relevance since, in most geotechnical problems, it is more interesting to estimate the peak and the residual shear resistance of interfaces before failure.

$$\begin{cases} \dfrac{\tau}{\sigma_n} = 0, & 0 \le u \le u_m \\ \dfrac{\tau}{\sigma_n} = k_s(u - u_m) = \dfrac{1}{\Delta u_p}\dfrac{\tau_p}{\sigma_n}(u - u_m), & u_m \le u \le u_p \\ \dfrac{\tau}{\sigma_n} = \dfrac{\tau_r}{\sigma_n} + \dfrac{\tau_p - \tau_r}{\sigma_n}\dfrac{u_p}{u}, & u \le u_p \end{cases} \quad (17)$$

where τ is the shear stress, τ_p is the peak shear strength, τ_r is the residual shear strength, σ_n is the normal stress, u is the shear displacement or horizontal displacement, u_m is the horizontal displacement to mate the two rock slabs during a direct shear test, u_p is the peak shear displacement, Δu_p is the horizontal displacement before the peak and k_s is the shear stiffness.

The problem of developing a methodology to estimate the overall shear responses of interfaces is addressed in this appendix. Differently from the model proposed by Grasselli and Egger (Grasselli and Egger 2003), the possibility of proposing an alternative constitutive model, which depends on the parameters used in failure criteria, is investigated. For this reason, a neural network model is evaluated to estimate the shear responses of concrete-rock interfaces submitted to lower normal loadings (0.5 and 1.5 MPa). The neural network model uses the database of shear responses of simulations of shear tests of synthetic concrete-rock interfaces (see section 3).

10.1.1 Prediction of the shear response of concrete-rock interfaces

The neural network model is set as a function f_{NN} which receives as input the normal stress (σ_n), the basic friction angle (Φ_b) and the roughness parameter $\theta^*_{max}/(C+1)$ and predicts the shear stress with the associated shear displacement $\left[[\delta_{s1}, \dots, \delta_{si}], [\tau_{s1}, \dots, \tau_{si}]\right]$, see Eq. (18).

$$f_{NN} : \left\{\sigma_n, \Phi_b, \frac{\theta^*_{max}}{(C+1)}\right\} \rightarrow \{[[\delta_{s1}, \dots, \delta_{si}], [\tau_{s1}, \dots, \tau_{si}]]\} \quad (18)$$

where τ_{si} is the shear stress at the instant "i" and δ_{si} is the associated shear displacement.

The dataset comprises 334 entries, each composed of the data relative to a single simulation of a shear test of the concrete-rock interface. The data of each simulation contains the normal stress (σ_n), the basic friction angle (Φ_b), the roughness parameter $\theta^*_{max}/(C+1)$ and a vector composed of 236 shear displacement values followed by 236 corresponding shear stress values.

The hyperparameter analysis is carried out to determine the suitable neural network architecture of the model. After hyperparameter analysis, the ideal neural network model for estimating the shear response of concrete-rock interfaces contains one input layer, six hidden layers, each with 25 neurons, and one output layer that yields a 472-long vector representing the shear displacement and the shear stress. The batch size of 8 entries is selected, and the neural network model is trained using 100 epochs.

10.1.2 Results of the neural network modeling to estimate the shear response of concrete-rock interfaces

10.1.2.1 Prediction of the peak shear strength using neural network model

The learning curve of the performance of the neural network model to estimate the shear response of concrete-rock interfaces is presented in Fig. 23. From this figure, it is clear that the evolution of the performance of the successive neural network models on the training and the validation dataset decreases with the increase in the number of epochs.

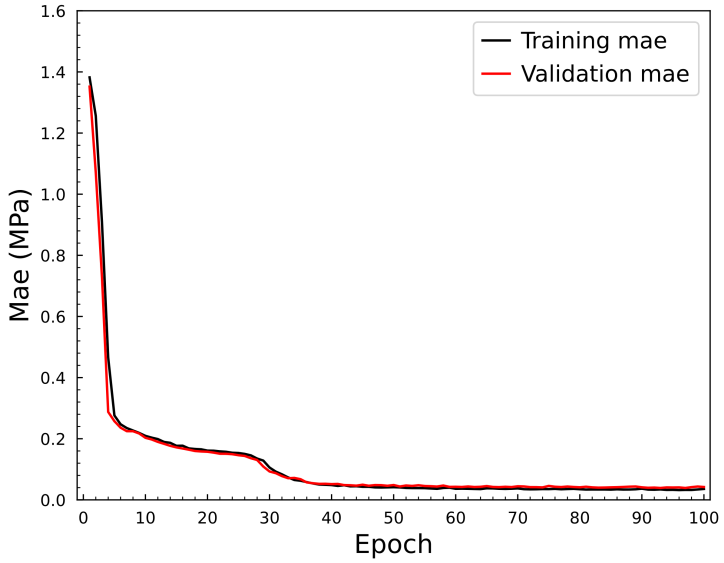

Fig. 23 Learning curve of the training of the neural network to estimate the shear response of concrete-rock interfaces

Fig. 24 presents the variation of the peak shear strengths extracted from shear responses predicted by the model in terms of the peak shear strength extracted from the shear response obtained using finite element simulations. A correlation coefficient of 0.95 and an MAE of 0.13 were obtained between the predicted and the simulated peak shear strength, proving that the shear response predicted by the neural network model can reproduce the peak shear strength obtained in the finite element simulation.

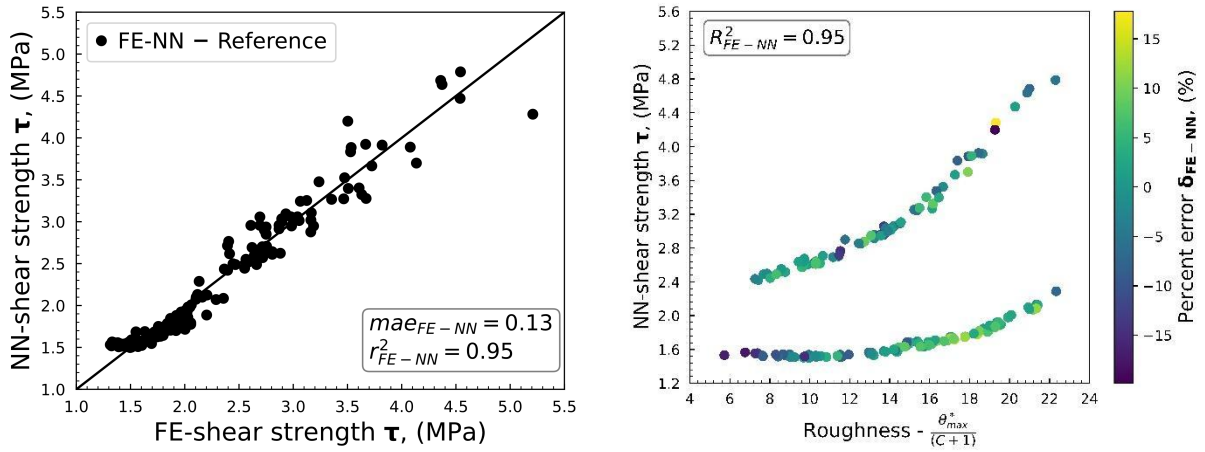

(a) **(b)**

Fig. 24 (a) Peak shear strength extracted from the predicted shear response obtained using neural network modeling (validation dataset) in terms of peak shear strength extracted from the shear response obtained using FE simulations and **(b)** percent error of **(a)**

10.1.2.2 Prediction of the peak shear strength obtained experimentally using neural network model

The experimental results used in this analysis are parts of the work performed by El Merabi (El Merabi 2018).

Fig. 25 presents the peak shear strength extracted from the shear response predicted by the neural network in terms of the peak shear strength obtained experimentally. A 0.96 correlation coefficient was obtained between the predicted and the experimentally obtained peak shear strength. However, this high correlation coefficient should be taken cautiously, given the size of the dataset.

10.1.2.3 Prediction of the shear response using the validation dataset

Examples of the neural network prediction of the shear responses of the direct shear test of concrete-rock interfaces using the validation dataset are presented in Fig. 26 and Fig. 27, along with the shear responses obtained using finite element simulations. From these figures, it is clear that the predicted shear response reproduces the three main stages of the shear evolution: the shear stress accumulation, the shear slip, and the residual shear stage. Furthermore, the peak and the residual peak shear strength obtained are close to their counterparts obtained via finite element simulations.

Furthermore, from Fig. 26 and Fig. 27, it is clear that the higher the roughness of the interface ($\theta^*_{max}/(C+1)$), the more resistant the interface. This observation highlights the influence of roughness on the shear response of concrete-rock interfaces when the normal stress is low.

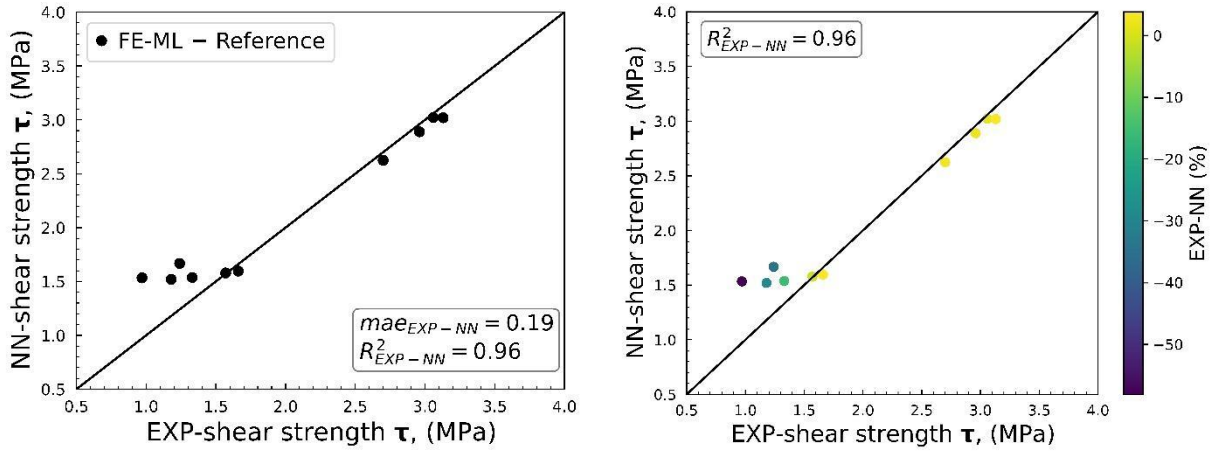

(a) **(b)**

Fig. 25 Peak **(a)** Peak shear strength extracted from the predicted shear response obtained using neural network modeling (Experimental) in terms of peak shear strength obtained experimental tests **(b)** percent error of **(a)**

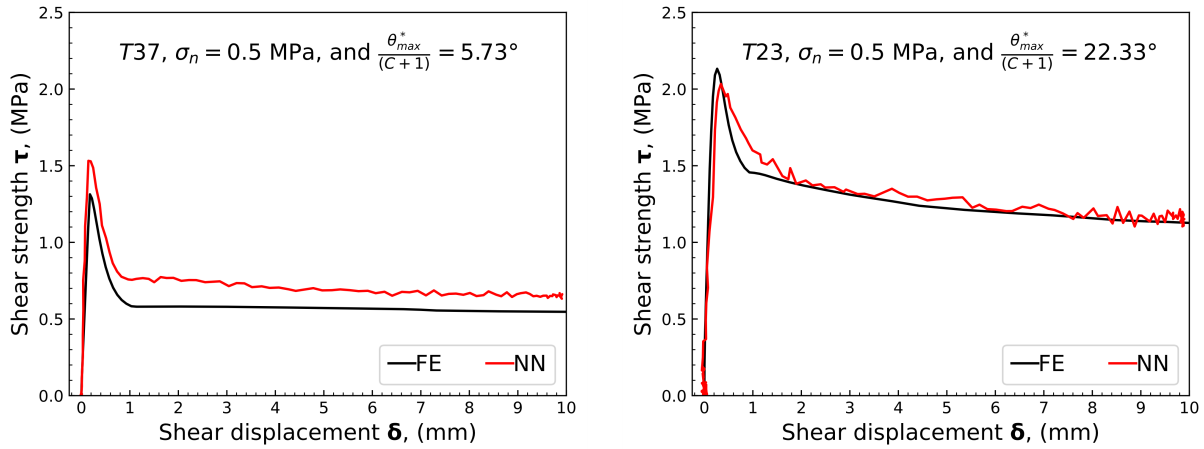

(a) **(b)**

Fig. 26 Comparison between the predicted and the numerically obtained shear responses of concrete-rock interfaces using NN and FE simulation: **(a)** T37 and **(b)** T26

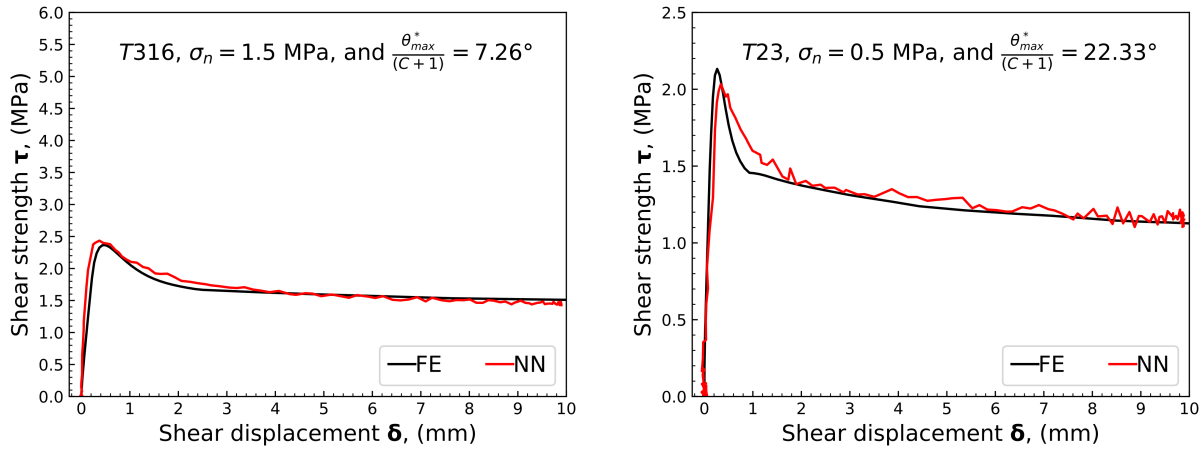

(a) **(b)**

Fig. 27 Comparison between the predicted and the numerically obtained shear responses of concrete-rock interfaces using NN and FE simulation: **(a)** T239 and **(b)** T261

10.1.2.4 Prediction of the shear response using the experimental data

The comparison between the shear responses predicted by the neural network and those obtained in experimental tests are presented in Fig. 28 to Fig. 32. Notably, the results of the experimental studies used in this analysis are part of the experimental campaign carried out by El Merabi (El Merabi 2018). These figures show that the predicted shear response captures the three parts of the shear evolutions and presents encouraging results in reproducing the peak and the residual shear strength of interfaces, which is interesting, given that the peak and the residual shear strength are predicted as single points of a 472-long vector.

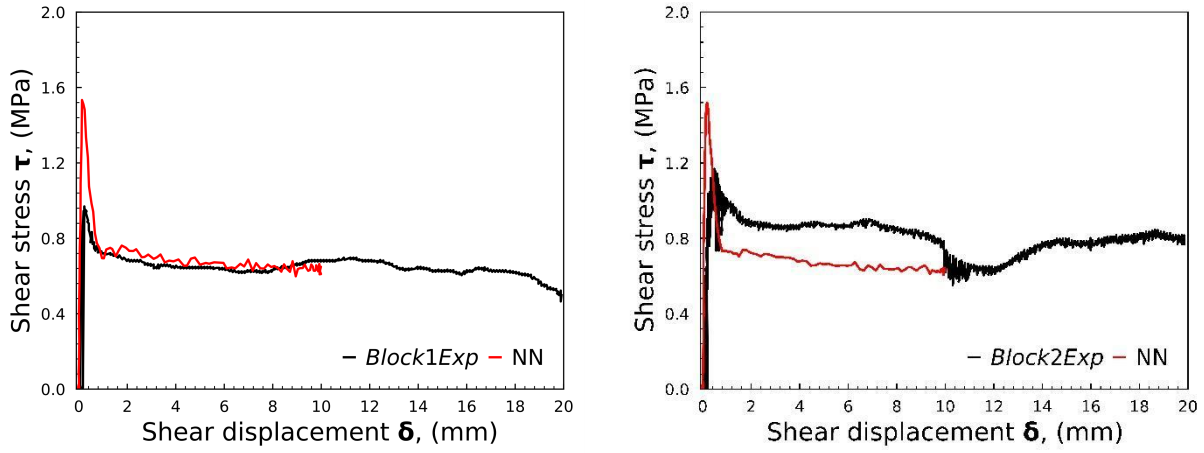

(a) **(b)**

Fig. 28 Comparison between the predicted and the experimentally obtained shear responses of concrete-rock interfaces using NN and tests: **(a)** Block 1 and **(b)** Block 2

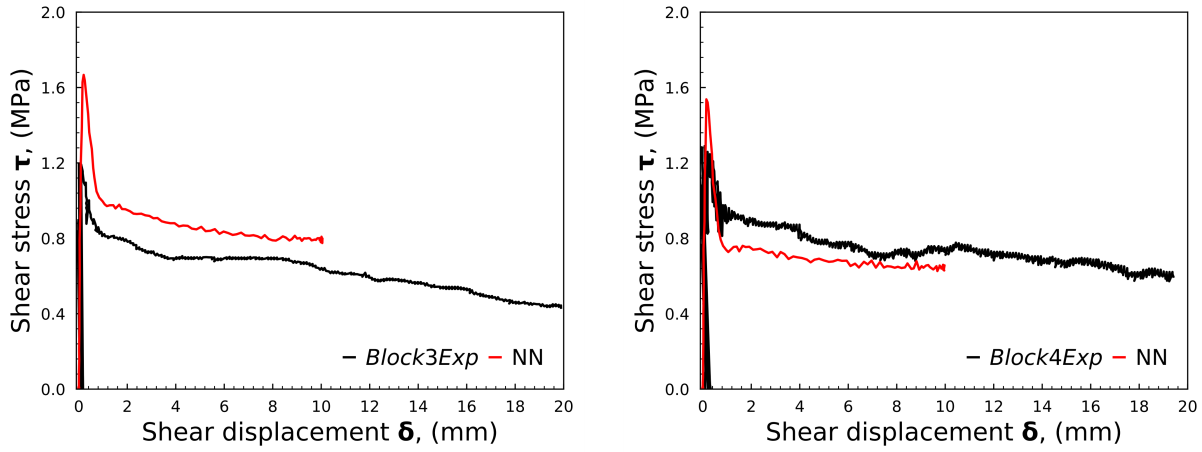

724 **Fig. 29** Comparison between the predicted and the experimentally obtained shear responses of concrete-rock
725 interfaces using NN and tests: **(a)** Block 3 and **(b)** Block 4

726

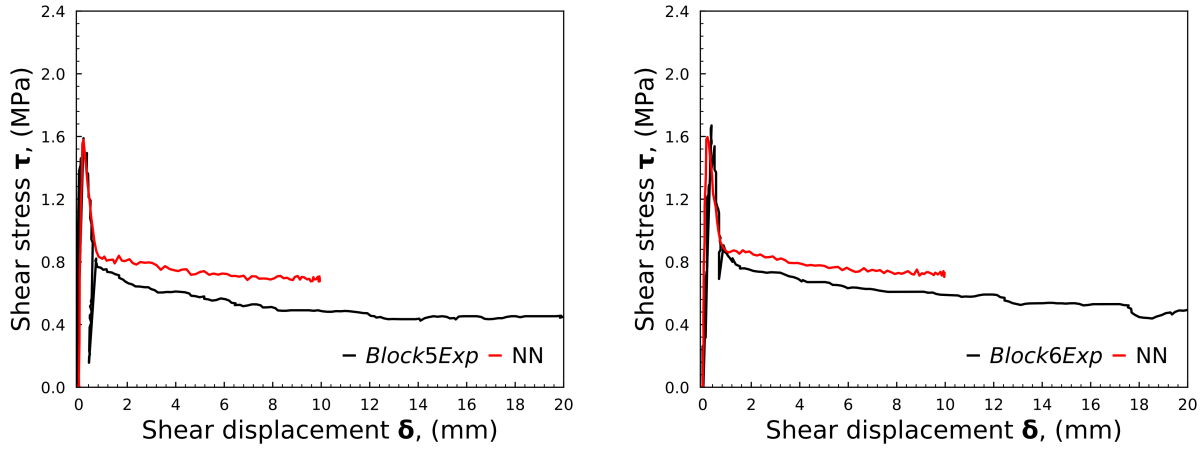

727 **Fig. 30** Comparison between the predicted and the experimentally obtained shear responses of concrete-rock
728 interfaces using NN and tests: **(a)** Block 5 and **(b)** Block 6

729

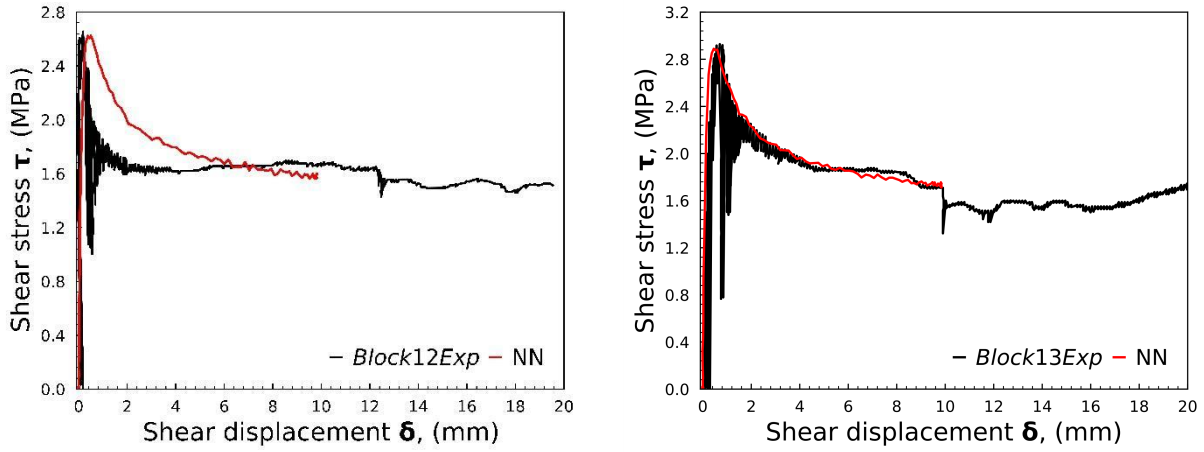

(a) **(b)**

Fig. 31 Comparison between the predicted and the experimentally obtained shear responses of concrete-rock interfaces using NN and tests: **(a)** Block 12 and **(b)** Block 13

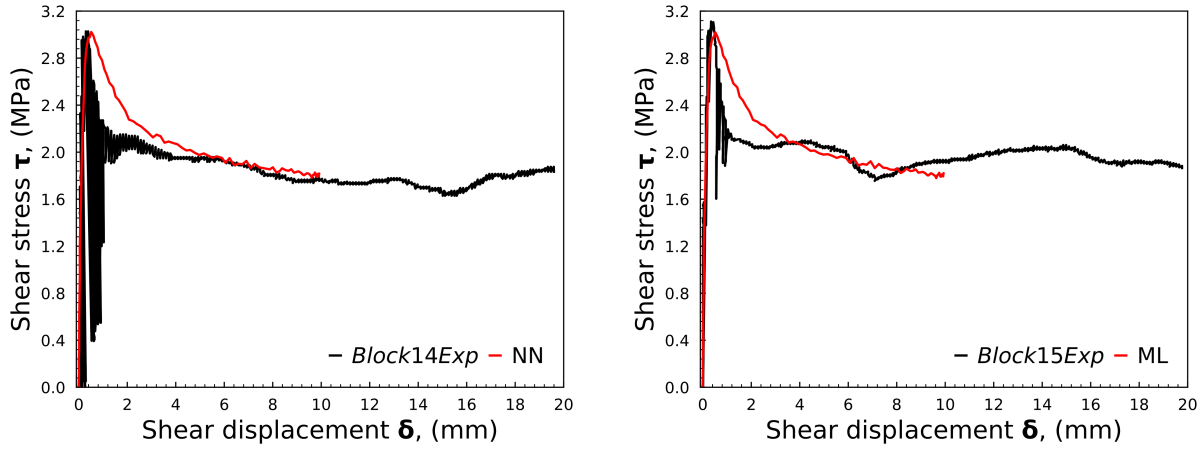

(a) **(b)**

Fig. 32 Comparison between the predicted and the experimentally obtained shear responses of concrete-rock interfaces using NN and tests: **(a)** Block 14 and **(b)** Block 15

Despite the interesting results obtained in the presented analysis on using neural network modeling to predict the overall shear response of concrete-rock interfaces, some questions remain. One such question is illustrated in Fig. 33, where the MAE seems to be very low when the entire shear response is used in the assessment (Fig. 33 legend Model) and is considerably high when only the peak shear strength extracted from the shear response is considered (Fig. 33 valPeak: validation, ExpPeak: experimental). This discrepancy could be addressed by defining a new evaluation metric that considers the two comparison scales (overall shear response and only the peak shear strength).

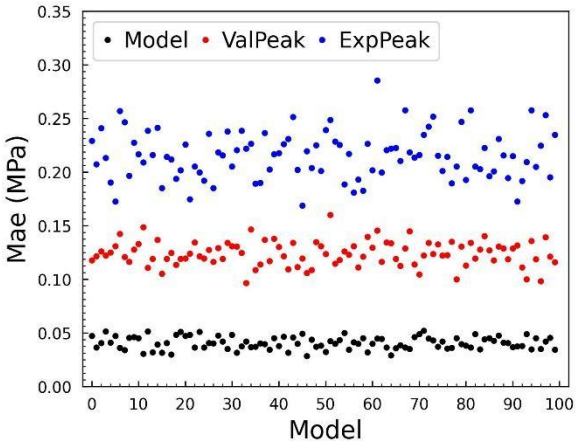

Fig. 33 Assessment of the MAE: computed using the comparison between the overall shear responses predicted and the FE shear responses obtained (model), calculated using the peak shear strength extracted from the predicted shear response and the peak shear strength obtained via FE simulation (validation) and Experimental tests (ExpPeak)

The result of this assessment sets the neural network modeling as a suitable methodology for estimating the shear strength and the shear responses of interfaces. However, it is important to highlight that improvement in the finite element simulations, the number and the variety of interfaces simulated, and the availability of more experimental results encompassing different types of rocks and different classes of roughness can increase the range of application of the neural network models.

11. Bibliography

Abadi, Martín, Ashish Agarwal, Paul Barham, Eugene Brevdo, Zhifeng Chen, Craig Citro, Greg S. Corrado, et al. 2016. "TensorFlow: Large-Scale Machine Learning on Heterogeneous Distributed Systems."

Amadei, B., J. Wibowo, S. Sture, and R. H. Price. 1998. "Applicability of Existing Models to Predict the Behavior of Replicas of Natural Fractures of Welded Tuff under Different Boundary Conditions." *Geotechnical and Geological Engineering* 16 (2): 79–128. https://doi.org/10.1023/A:1008886106337.

Badika, Menes, Bassel El Merabi, Sophie Capdevielle, Frederic Dufour, Dominique Saletti, and Matthieu Briffaut. 2022. "Influence of Concrete–Rock Bonds and Roughness on the Shear Behavior of Concrete–Rock Interfaces under Low Normal Loading, Experimental and Numerical Analysis." *Applied Sciences* 12 (11): 5643. https://doi.org/10.3390/app12115643.

Bandis, S., A.C. Lumsden, and N.R. Barton. 1981. "Experimental Studies of Scale Effects on the Shear Behaviour of Rock Joints." *International Journal of Rock Mechanics and Mining Sciences & Geomechanics Abstracts* 18 (1): 1–21. https://doi.org/10.1016/0148-9062(81)90262-X.

Barton, N., and V. Choubey. 1977. "The Shear Strength of Rock Joints in Theory and Practice." *Rock Mechanics Felsmechanik Mecanique Des Roches* 10 (1–2): 1–54. https://doi.org/10.1007/BF01261801.

Boulon, M. 1995. "A 3-D Direct Shear Device for Testing the Mechanical Behaviour and the Hydraulic Conductivity of Rock Joints." In *Proceedings of the Second International Conference on Mechanics of Jointed and Faulted Rock MJFR-2*, 407–413. Vienna, Austria.

Casagrande, D., O. Buzzi, A. Giacomini, C. Lambert, and G. Fenton. 2018. *A New Stochastic Approach to Predict Peak and Residual Shear Strength of Natural Rock Discontinuities*. *Rock Mechanics and Rock Engineering*. Vol. 51. Springer Vienna. https://doi.org/10.1007/s00603-017-1302-3.

Chilès, Jean-Paul, and Pierre Delfiner. 2012. *Geostatistics*. Wiley Series in Probability and Statistics. Wiley. https://doi.org/10.1002/9781118136188.

Chollet, François. 2021. *Deep Learning with Python*. Second Edi. Manning.

Dantas Neto, Silvrano Adonias, Buddhima Indraratna, David Américo Fortuna Oliveira, and André Pacheco de Assis. 2017. "Modelling the Shear Behaviour of Clean Rock Discontinuities Using Artificial Neural Networks." *Rock Mechanics and Rock Engineering* 50 (7): 1817–31. https://doi.org/10.1007/s00603-017-1197-z.

Delavar, Mohammad Reza, and Ahmad Ramezanzadeh. 2023. "Pore Pressure Prediction by Empirical and Machine Learning Methods Using Conventional and Drilling Logs in Carbonate Rocks." *Rock Mechanics and Rock Engineering* 56 (1): 535–64. https://doi.org/10.1007/s00603-022-03089-y.

Deutsch, C. V., and A. G. Journel. 1998. "GSLIB: Geostatistical Software Library and User's Guide. Second Edition." *GSLIB: Geostatistical Software Library and User's Guide. Second Edition*.

El-Soudani, S.M. 1978. "Profilometric Analysis of Fractures." *Metallography* 11 (3): 247–336. https://doi.org/10.1016/0026-0800(78)90045-9.

Emery, Xavier, and Christian Lantuéjoul. 2006. "TBSIM: A Computer Program for Conditional Simulation of Three-Dimensional Gaussian Random Fields via the Turning Bands Method." *Computers and Geosciences* 32 (10): 1615–28. https://doi.org/10.1016/j.cageo.2006.03.001.

Fenton, Gordon A., and D. V. Griffiths. 2008. *Risk Assessment in Geotechnical Engineering*. *Risk Assessment in Geotechnical Engineering*. https://doi.org/10.1002/9780470284704.

Fenton, Gordon A., and Erik H. Vanmarcke. 1990. "Simulation of Random Fields via Local Average Subdivision." *Journal of Engineering Mechanics* 116 (8): 1733–49. https://doi.org/10.1061/(ASCE)0733-9399(1990)116:8(1733).

Furtney, J. K., C. Thielsen, W. Fu, and R. Le Goc. 2022. "Surrogate Models in Rock and Soil Mechanics: Integrating Numerical Modeling and Machine Learning." *Rock Mechanics and Rock Engineering* 55 (5): 2845–59. https://doi.org/10.1007/s00603-021-02720-8.

Grasselli, G., and P. Egger. 2003. "Constitutive Law for the Shear Strength of Rock Joints Based on Three-Dimensional Surface Parameters." *International Journal of Rock Mechanics and Mining Sciences* 40 (1): 25–40. https://doi.org/10.1016/S1365-1609(02)00101-6.

Hoek, Evert, and Edwin T. Brown. 1980. "Empirical Strength Criterion for Rock Masses." *Journal of the Geotechnical Engineering Division* 106 (9): 1013–35. https://doi.org/10.1061/AJGEB6.0001029.

Jahed Armaghani, Danial, Mohd For Mohd Amin, Saffet Yagiz, Roohollah Shirani Faradonbeh, and Rini Asnida Abdullah. 2016. "Prediction of the Uniaxial Compressive Strength of Sandstone Using Various Modeling Techniques." *International Journal of Rock Mechanics and Mining Sciences* 85 (May): 174–86. https://doi.org/10.1016/j.ijrmms.2016.03.018.

Jeffery, M., J. Huang, S. Fityus, A. Giacomini, and O. Buzzi. 2021. "A Rigorous Multiscale Random Field Approach to Generate Large Scale Rough Rock Surfaces." *International Journal of Rock Mechanics and Mining Sciences* 142 (June): 104716. https://doi.org/10.1016/j.ijrmms.2021.104716.

Journel, A. G, and Ch J Huijbregts. 1976. *Mining Geostatistics*. *London: Academic*. United Kingdom.

Khandelwal, Manoj, and T.N. Singh. 2009. "Prediction of Blast-Induced Ground Vibration Using Artificial Neural Network." *International Journal of Rock Mechanics and Mining Sciences* 46 (7): 1214–22. https://doi.org/10.1016/j.ijrmms.2009.03.004.

Kingma, Diederik P., and Jimmy Lei Ba. 2015. "Adam: A Method for Stochastic Optimization." *3rd International Conference on Learning Representations, ICLR 2015 - Conference Track Proceedings*, 1–15.

Krizhevsky, Alex, Ilya Sutskever, and Geoffrey E Hinton. 2017. "ImageNet Classification with Deep Convolutional Neural Networks." *COMMUNICATIONS OF THE ACM* 60 (6). https://doi.org/10.1145/3065386.

Ladany, B., and G. Archambault. 1969. “Simulation of Shear Behavior of a Jointed Rock Mass,” no. January 1969: 105–25.

Liu, Quansheng, Yongchao Tian, Dongfeng Liu, and Yalong Jiang. 2017. “Updates to JRC-JCS Model for Estimating the Peak Shear Strength of Rock Joints Based on Quantified Surface Description.” *Engineering Geology* 228 (October): 282–300. https://doi.org/10.1016/j.enggeo.2017.08.020.

Mantoglou, Aristotelis, and John L. Wilson. 1982. “The Turning Bands Method for Simulation of Random Fields Using Line Generation by a Spectral Method.” *Water Resources Research* 18 (5): 1379–94. https://doi.org/10.1029/WR018i005p01379.

Matheron, G. 1973. “The Intrinsic Random Functions and Their Applications.” *Advances in Applied Probability* 5 (3): 439–68. https://doi.org/10.2307/1425829.

Merabi, Bassel El. 2018. “Mechanical Behavior of Cohesive Concrete-Rock Joints at the Dam-Foundation Interface : Geometrical and Mechanical Influence of Asperities.” Université Grenoble Alpes. https://theses.hal.science/tel-01783168.

Meulenkamp, F., and M.Alvarez Grima. 1999. “Application of Neural Networks for the Prediction of the Unconfined Compressive Strength (UCS) from Equotip Hardness.” *International Journal of Rock Mechanics and Mining Sciences* 36 (1): 29–39. https://doi.org/10.1016/S0148-9062(98)00173-9.

Moradian, Z. A., G. Ballivy, P. Rivard, C. Gravel, and B. Rousseau. 2010. “Evaluating Damage during Shear Tests of Rock Joints Using Acoustic Emissions.” *International Journal of Rock Mechanics and Mining Sciences* 47 (4): 590–98. https://doi.org/10.1016/j.ijrmms.2010.01.004.

Moradian, Z.A., G. Ballivy, and P. Rivard. 2012. “Application of Acoustic Emission for Monitoring Shear Behavior of Bonded Concrete–Rock Joints under Direct Shear Test.” *Canadian Journal of Civil Engineering* 39 (8): 887–96. https://doi.org/10.1139/l2012-073.

Mouzannar, Hussein. 2016. “Caractérisation de La Résistance Au Cisaillement et Comportement Des Interfaces Entre Béton et Fondation Rocheuse Des Structures Hydrauliques.” Université de Lyon.

Mouzannar, Hussein, Marion Bost, Madly Leroux, and Didier Virely. 2017. “Experimental Study of the Shear Strength of Bonded Concrete–Rock Interfaces: Surface Morphology and Scale Effect.” *Rock Mechanics and Rock Engineering* 50 (10): 2601–25. https://doi.org/10.1007/s00603-017-1259-2.

Myers, N.O. 1962. “Characterization of Surface Roughness.” *Wear* 5 (3): 182–89. https://doi.org/10.1016/0043-1648(62)90002-9.

Patton, F. D. 1966. “Multiple Modes of Shear Failure in Rock.” *1st ISRM Congress 1966*, 509–13.

Plesha, Michael E. 1987. “Constitutive Models for Rock Discontinuities with Dilatancy and Surface Degradation.” *International Journal for Numerical and Analytical Methods in Geomechanics* 11 (4): 345–62. https://doi.org/10.1002/nag.1610110404.

Pyrcz, Michael J., and Clayton V. Deutsch. 2020. “Transforming Data to a Gaussian Distribution.” *Geostatistics Lessons*, 1–4.

Rabbani, E., F. Sharif, M. Koolivand Salooki, and A. Moradzadeh. 2012. “Application of Neural Network Technique for Prediction of Uniaxial Compressive Strength Using Reservoir Formation Properties.” *International Journal of Rock Mechanics and Mining Sciences* 56 (December): 100–111. https://doi.org/10.1016/j.ijrmms.2012.07.033.

Rajesh Kumar, B., Harsha Vardhan, M. Govindaraj, and G.S. Vijay. 2013. “Regression Analysis and ANN Models to Predict Rock Properties from Sound Levels Produced during Drilling.” *International Journal of Rock Mechanics and Mining Sciences* 58 (February): 61–72. https://doi.org/10.1016/j.ijrmms.2012.10.002.

Rukhaiyar, S., and N.K. Samadhiya. 2017. “A Polyaxial Strength Model for Intact Sandstone Based on Artificial Neural Network.” *International Journal of Rock Mechanics and Mining Sciences* 95 (May): 26–47. https://doi.org/10.1016/j.ijrmms.2017.03.012.

Rullière, Adrien, Patrice Rivard, Laurent Peyras, and Pierre Breul. 2020. “Influence of Roughness on the Apparent Cohesion of Rock Joints at Low Normal Stresses.” *Journal of Geotechnical and Geoenvironmental Engineering* 146 (3). https://doi.org/10.1061/(ASCE)GT.1943-5606.0002200.

Saiang, D., L. Malmgren, and E. Nordlund. 2005. “Laboratory Tests on Shotcrete-Rock Joints in Direct Shear, Tension and Compression.” *Rock Mechanics and Rock Engineering* 38 (4): 275–97. https://doi.org/10.1007/s00603-005-0055-6.

Sakaridis, Emmanouil, Nikolaos Karathanasopoulos, and Dirk Mohr. 2022. “Machine-Learning Based Prediction of Crash Response of Tubular Structures.” *International Journal of Impact Engineering* 166 (August). https://doi.org/10.1016/j.ijimpeng.2022.104240.

Samson, Matthew, and Clayton V Deutsch. 2021. “The Sill of the Variogram,” 1–6.

Tatone, B. S.A., G. Grasselli, and B. Cottrell. 2010. “Accounting for the Influence of Measurement Resolution on Discontinuity Roughness Estimates.” *Rock Mechanics in Civil and Environmental Engineering - Proceedings of the European Rock Mechanics Symposium, EUROCK 2010*, no. March: 203–6. https://doi.org/10.1201/b10550-45.

Tatone, Bryan S. A., and Giovanni Grasselli. 2009. “A Method to Evaluate the Three-Dimensional Roughness of Fracture Surfaces in Brittle Geomaterials.” *Review of Scientific Instruments* 80 (12): 125110. https://doi.org/10.1063/1.3266964.

Tian, H. M., W. Z. Chen, D. S. Yang, and J. P. Yang. 2015. “Experimental and Numerical Analysis of the Shear Behaviour of Cemented Concrete–Rock Joints.” *Rock Mechanics and Rock Engineering* 48 (1): 213–22. https://doi.org/10.1007/s00603-014-0560-6.

Wackernagel, Hans. 2003. *Multivariate Geostatistics*. Berlin, Heidelberg: Springer Berlin Heidelberg. https://doi.org/10.1007/978-3-662-05294-5.

Whitehouse, David J. 2023. *Handbook of Surface Metrology*. 1st editio. Boca Raton: Routledge. https://doi.org/10.1201/9780203752609.

Yesiloglu-Gultekin, N., C. Gokceoglu, and E.A. Sezer. 2013. “Prediction of Uniaxial Compressive Strength of Granitic Rocks by Various Nonlinear Tools and Comparison of Their Performances.” *International Journal of Rock Mechanics and Mining Sciences* 62 (September): 113–22. https://doi.org/10.1016/j.ijrmms.2013.05.005.

Zhao, Wusheng, Weizhong Chen, and Kun Zhao. 2018. “Laboratory Test on Foamed Concrete-Rock Joints in Direct Shear.” *Construction and Building Materials* 173 (June): 69–80. https://doi.org/10.1016/j.conbuildmat.2018.04.006.